

ERDC/CERL TR-02-33

Construction Engineering
Research Laboratory

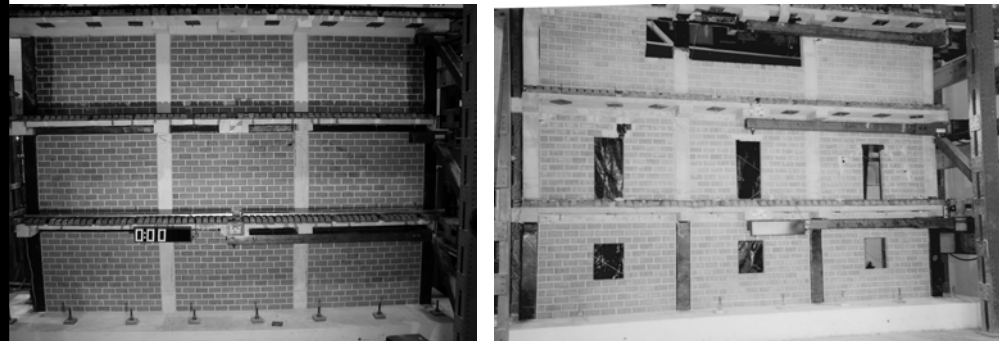


US Army Corps
of Engineers®
Engineer Research and
Development Center

Design of Fiber-Reinforced Polymer Materials for Seismic Rehabilitation of Infilled Concrete Structures

Ghassan K. Al-Chaar and Gregory E. Lamb

December 2002



Foreword

This study was conducted for Headquarters, U.S. Army Corps of Engineers (USACE) under project 622784AT41, “Military Facilities Engineering Technologies (6.2 Exploratory Development),” PROMIS No. CFM-A011, “Seismic Rehabilitation of Concrete Frames with Infill.” The technical monitor was David C. Bohl, CECW-EW.

The work was performed by the Materials and Structures Branch (CF-M) of the Facilities Division (CF), Construction Engineering Research Laboratory (CERL). The CERL Principal Investigator was Dr. Ghassan Al-Chaar. The technical editors were Gordon L. Cohen and Linda L. Wheatley, Information Technology Laboratory — Champaign. Martin J. Savoie is Chief, CF-M, and L. Michael Golish is Chief, CF. The Technical Director of the Facilities Acquisition and Rehabilitation business area was Dr. Paul A. Howdysshell, and the Director of CERL is Dr. Alan W. Moore.

The author wishes to thank Dr. Dan P. Abrams for his review and input for this research project, Dr. Richard Klingler for his input, and the COE Seismic Review Panelists Joseph P. Hartman, HQ02, Ghassem Khosrownia, SPK, Thomas D. Wright, NWK, and David C. Bohl, HQ02, for the technical guidelines of the project. Thanks also go to the Seismic and Structural Engineering team members Dr. John R. Hayes, Jr. and Steven C. Sweeney for their review and input.

CERL is an element of the Engineer Research and Development Center (ERDC), U.S. Army Corps of Engineers. The Commander and Executive Director of ERDC is COL John W. Morris III, EN, and the Director is Dr. James R. Houston.

DISCLAIMER: The contents of this report are not to be used for advertising, publication, or promotional purposes. Citation of trade names does not constitute an official endorsement or approval of the use of such commercial products. All product names and trademarks cited are the property of their respective owners. The findings of this report are not to be construed as an official Department of the Army position unless so designated by other authorized documents.

DESTROY THIS REPORT WHEN IT IS NO LONGER NEEDED. DO NOT RETURN IT TO THE ORIGINATOR.

Contents

Foreword	2
List of Figures and Tables	5
1 Introduction	7
Background.....	7
Objective	8
Approach	8
Scope.....	8
Mode of Technology Transfer	8
Units of Weight and Measure	9
2 Determining the Geometrical and Mechanical Properties of Masonry and FRP Structural Components	10
Introduction	10
Panel Material Properties	10
Characteristics of FRP Systems	11
<i>As-Installed Properties</i>	11
<i>Environmental Reduction Factor (C_E)</i>	13
<i>FRP Stress-Strain Relationship</i>	14
3 Load and Deformation Characteristics of FRP-Rehabilitated R/C Frames	15
Failure Modes	15
Flexural Capacity of Rehabilitated Frame Members	15
<i>Assumptions</i>	15
<i>Flexural Design</i>	17
<i>Moment-Curvature Behavior of Rehabilitated Frame Members</i>	20
Shear Capacity of Rehabilitated Frame Members.....	22
Axial Compressive and Tensile Strength of Rehabilitated Frame Members	25
Moment-Thrust Interaction of Rehabilitated Frame Members	27
4 In-Plane Strength Evaluation of URM Infill Rehabilitated With FRP	29
Background.....	29
General Evaluation Procedure Using Pushover Analyses	30
<i>Equivalent Strut Width</i>	31
<i>Eccentricity of Equivalent Strut</i>	34
<i>Partially Infilled Frames</i>	35
<i>Perforated Panels</i>	35
<i>Existing Infill Damage</i>	37
<i>Infill Rehabilitated With FRP</i>	38
<i>Load-Deformation Behavior of the Eccentric Equivalent Strut</i>	39

<i>Plastic Hinge Placement</i>	42
<i>Rigid End Offsets</i>	44
<i>Loading</i>	44
5 In-Plane Stiffness Evaluation of URM Infill Rehabilitated With FRP	45
Bilinear Load-Deflection Behavior	45
Determination of K_i and K_f	47
6 Summary	50
References	51
Appendix A: 3x3 Full-Scale Example	54
Appendix B: Commentary on Selected Sections.....	67
Glossary	74
CERL Distribution	82
Report Documentation Page	83

List of Figures and Tables

Figures

1	Stress-strain curve for a +45 / -45 degree carbon FRP coupon	12
2	Bilinear FRP stress-strain curve.....	13
3	FRP design strength curve.....	14
4	Effectiveness of FRP in flexure and the recommended FRP wrapping scheme	17
5	Stress and strain distribution at ultimate load	17
6	Bond-dependent coefficient, κ_m , for flexure	19
7	Strength reduction factor, ϕ	20
8	Simplified moment-curvature relationship.....	21
9	Stress-strain distribution at M_y	21
10	Effectiveness of FRP in shear and the recommended wrapping scheme	23
11	Variables used in shear strength calculations.....	23
12	Illustration of the variable r	27
13	Moment-thrust interaction curve.....	28
14	Specimen deformation shape.....	32
15	Equivalent diagonal strut.....	33
16	Strut geometry	33
17	Placement of strut	35
18	Partially infilled frame	35
19	Perforated panel.....	36
20	Possible strut placement for perforated panel.....	37
21	Visual damage classification	38
22	FRP Strip Orientation used on Masonry Walls.....	39
23	Geometry of θ_{strut}	40
24	Load-deformation behavior	40
25	Shear failure of masonry	42
26	Distance to beam hinge.....	43
27	Plastic hinge placement	43
28	Rigid end offset placement.....	44
29	Bilinear load-deflection curve	46

30	Modified load-deflection curve	46
31	Upper / lower limit strut width	47

Tables

1	Composite FRP system properties	12
2	Values of C_E for different FRP systems	13
3	Values of ψ_f for flexural strengthening	18
4	Values of ψ_f for shear strengthening	22
5	In-plane damage reduction factor	37
6	FRP strength increase factors	39
7	FRP stiffness increase factors	41

1 Introduction

Background

A recent study by the U.S. Army Engineer Research and Development Center (ERDC), Construction Engineering Research Laboratory (CERL) for the Federal Emergency Management Agency (FEMA) revealed that more than half of the Army buildings located in high or moderate seismic zones did not meet current seismic code requirements and were found vulnerable to damage during an earthquake. One rehabilitation technique that addresses vulnerabilities in both the masonry infills and in nonductile concrete frames is the use of fiber-reinforced polymer (FRP). ERDC/CERL investigated the effectiveness of such a technique by conducting an experimental program on reinforced concrete (R/C) frames infilled with masonry. Based on this research and related research in the field, this report was developed to provide in-depth guidelines for engineers and practitioners on how to evaluate the strength and stiffness of R/C members and masonry-infilled frames strengthened with FRP.

This document uses the same nomenclature used in ACI 440, *Guide for the Design and Construction of Externally Bonded FRP Systems for Strengthening Concrete Structures*, when possible. Major contributions that go beyond ACI 440 include guidance on:

- FRP systems that have nonlinear stress-strain behavior
- flexural strength of R/C members fully wrapped with FRP and containing compression steel reinforcement
- moment-curvature relationships for beams
- compressive strength of noncircular R/C members
- thrust-moment interaction behavior for columns
- strength and stiffness of masonry-infilled frames with FRP overlay
- global structural system performance evaluation using nonlinear pushover analysis.

Objective

The objective of this project was to present guidelines for evaluating strength and stiffness of unreinforced masonry (URM) infill panels rehabilitated with FRP and subjected to lateral forces. The guidelines are based on experimental and computational research performed at ERDC, and they include a number of empirically based relationships for estimating strength and stiffness of infill panels subjected to lateral forces. The guidelines give the engineer a strength-based alternative to FEMA 273 (a performance-based method), which should also result in safe and economical construction.

Approach

The information compiled in this report was written following a logical sequence intended to help the engineer in the evaluation process. First, the following chapter outlines the steps that must be followed to obtain all the required material and geometrical properties of the structure to be evaluated. In the next chapters, the load and deformation characteristics of R/C members strengthened with FRP are presented. Next, the in-plane strength and stiffness evaluation procedures are shown for the lateral-force resisting system consisting of infilled frames rehabilitated with FRP. Appendix A includes an illustrative example to help summarize and clarify the entire evaluation process, and Appendix B is a commentary on selected sections of the document.

Scope

The evaluation procedures presented in this document (based on life-safety performance) are applicable to all building structures that have been constructed with R/C frames and walls that consist of infill panels constructed of solid clay brick, concrete block, and hollow clay tile masonry. These types of structures correspond to Building type 10 as defined in Chapter 2 and in accordance with FEMA 310.

Mode of Technology Transfer

This report is to be used as a complement to applicable provisions in FEMA 310 with respect to seismic evaluation of buildings.

Units of Weight and Measure

U.S. standard units of measure are used throughout this report. A table of conversion factors for Standard International (SI) units is provided below.

SI conversion factors		
1 in.	=	2.54 cm
1 sq in.	=	6.452 cm ²
1 lb	=	0.453 kg
1 kip	=	453 kg
1 psi	=	6.89 kPa

2 Determining the Geometrical and Mechanical Properties of Masonry and FRP Structural Components

Introduction

The general requirements presented in Chapter 2 of ERDC/CERL TR-02-1, *Evaluating Strength and Stiffness of Unreinforced Masonry Infill Structures* (Al-Chaar 2002), are applicable in this document. All geometrical properties, including the size and location of all masonry infills and confining frame elements, should be determined. Infill dimensions such as height (h), length (l), and thickness (t) should be obtained from field measurements or existing construction/structural plans. All relevant dimensions for the frame elements (H , L_f , h_b , b_b , h_c , b_c , etc.) must also be obtained. Definitions of these dimensions are given in the glossary.

Panel Material Properties

Tests required to evaluate mechanical material properties of the masonry infills such as compressive strength (f'_m), modulus of elasticity in compression (E_m), and shear strength (f'_v) must be carried out in accordance with Section 7.3.2 (Properties of In-Place Materials) of FEMA 273, *NEHRP Guidelines for the Seismic Rehabilitation of Buildings*. Evaluation of material properties for the confining frame should be executed in accordance with Section 6.3.2 (for R/C frames) of FEMA 273. Evaluation of material properties of the FRP should be consistent with Chapters 3 and 6 of ACI 440. Material properties may also be obtained from building codes from the year of construction of the building being evaluated, or from as-built plans if available.

Masonry infill panels should be evaluated in both the in-plane and out-of-plane direction while accounting for the effects of out-of-plane loading on in-plane capacity. In general, infills can be grouped into two different categories: (1) isolated infills and (2) shear (or regular) infills.

Isolated infills are panels totally isolated from the confining frame at the top and on both sides. The isolation (gaps) between the infill and the frame must be greater than any possible deformation expected by the frame, thus prohibiting any infill/frame interaction. These infills are not considered structural elements.

This report focuses on *shear infills*, which act as part of the lateral-force-resisting system of the structure. An infill in this category must be fully in tight contact with its confining frame on all four of its sides. Any gaps must be completely filled to guarantee full mortar bonding contact.

In-plane and out-of-plane behavior of infilled frames depends on a number of factors outside of the basic mechanical and geometrical properties of the infill and frame. These additional factors alter the original stiffness and strength of infilled frames. The empirically developed factors presented in this report modify original infilled frame performance estimates by taking into account existing infill damage, flexibility of confining frame elements, and presence of infill openings. In addition, factors representing the influence of FRP overlay used as a rehabilitation technique are presented. These multiplicative factors will be discussed in later sections.

Characteristics of FRP Systems

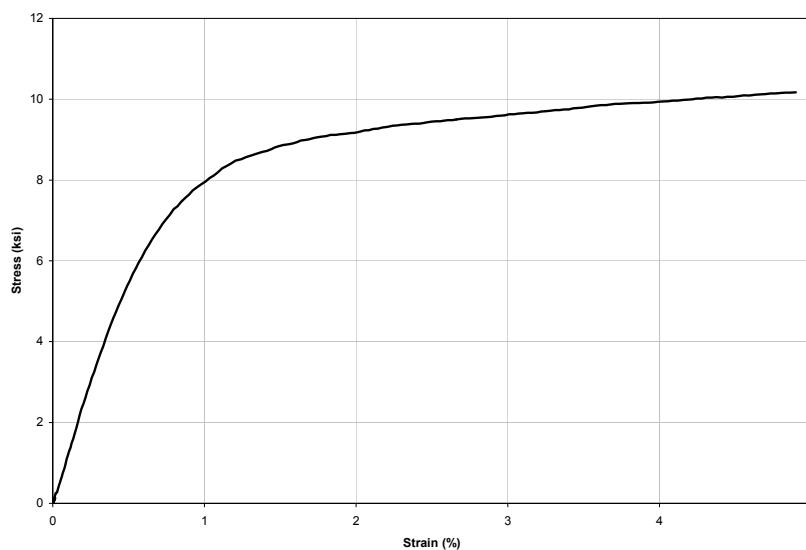
As-Installed Properties

The as-installed structural properties of the FRP systems vary considerably with the type of fiber and fiber orientation. Table 1 summarizes the composite tensile properties of FRP systems with fiber volumes of 40 – 60 percent (ACI 440). The symbol E_f refers to the initial modulus of elasticity of the FRP system, f_{fu}^* is the ultimate tensile strength of the FRP system, and ϵ_f^* is the ultimate rupture strain of the FRP system. The properties are based on the gross laminate area rather than using just the net fiber area.

Table 1. Composite FRP system properties.

FRP System	Fiber Orientation	E_{fl} (10^3 ksi)	f_{fu}^* (ksi)	ϵ_{fu}^* (%)
High Strength Carbon/Epoxy	0°	15 - 21	150 - 350	1.0 - 1.5
	$0^\circ/90^\circ$	8 - 11	100 - 150	1.0 - 1.5
	$+45^\circ/-45^\circ$	2 - 4	25 - 40	1.5 - 2.5
E-glass/Epoxy	0°	3 - 6	75 - 200	1.5 - 3.0
	$0^\circ/90^\circ$	2 - 5	75 - 150	2.0 - 3.0
	$+45^\circ/-45^\circ$	2 - 3	25 - 40	2.5 - 3.5
High Performance Aramid/Epoxy	0°	7 - 10	100 - 250	2.0 - 3.0
	$0^\circ/90^\circ$	4 - 5	40 - 80	2.0 - 3.0
	$+45^\circ/-45^\circ$	1 - 2	20 - 30	2.0 - 3.0

Traditionally, engineers have assumed linearly elastic behavior until failure for the FRP. This assumption is valid for FRP systems with fiber orientations of zero degrees and $0/90$ degrees. FRP systems with fiber orientations of $+45/-45$ degrees, however, may exhibit highly nonlinear response. Figure 1 illustrates, for example, the nonlinear stress-strain characteristics for a tensile test of a carbon FRP (CFRP) coupon with the fibers oriented $+45/-45$.

**Figure 1. Stress-strain curve for a $+45/-45$ degree CFRP coupon.**

Therefore, the structural properties of the FRP system should be determined from testing on the specific fiber/resin combination being used. Once an average stress-strain curve has been generated, a bilinear representation can be utilized for design purposes. The bilinear curve should be drawn in a manner that minimizes the deviations from the actual stress-strain curve. Figure 2 shows a typical bilinear FRP stress-strain curve.

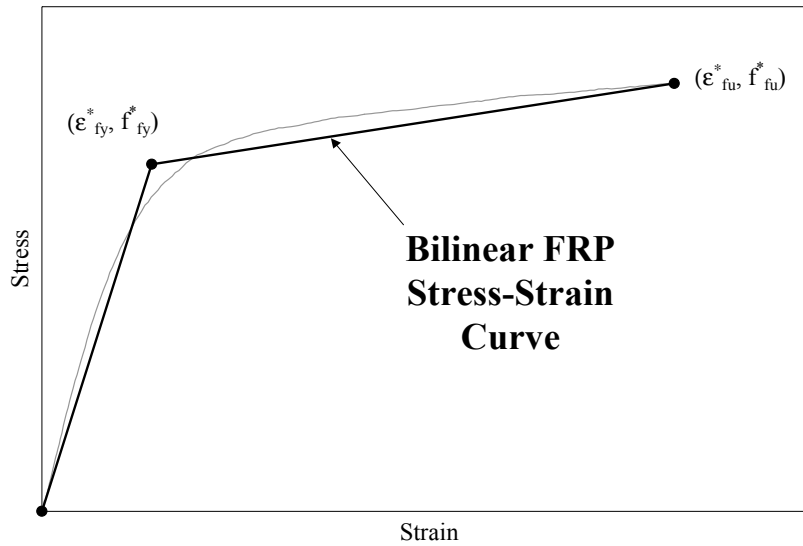


Figure 2. Bilinear FRP stress-strain curve.

Environmental Reduction Factor (C_E)

The properties of the FRP system determined from testing should only be considered initial values. After FRP is exposed to the environment for long durations of time, the strength decreases. Table 2 gives conservative values for the environmental reduction factor, C_E , for different environmental exposure conditions and fiber/resin combinations. The aggressive environmental exposure values should be used when the FRP system will be subjected to high humidity, freeze-thaw cycles, salt water, or alkalinity (ACI 440).

Table 2. Values of C_E for different FRP systems.

Environmental Exposure	FRP System	C_E
Interior	Carbon/Epoxy	0.95
	Glass/Epoxy	0.75
	Aramid/Epoxy	0.85
Exterior	Carbon/Epoxy	0.85
	Glass/Epoxy	0.65
	Aramid/Epoxy	0.75
Aggressive	Carbon/Epoxy	0.85
	Glass/Epoxy	0.5
	Aramid/Epoxy	0.7

The environmental reduction factor should be applied to the yield stress, ultimate stress, yield strain, and ultimate strain of the FRP system determined from testing. Therefore, the design strength of the FRP system is reduced without modifying the

modulus values. The following equations give the tensile properties that should be used in design (Eq 1).

$$\begin{aligned} f_{fy} &= C_E f_{fy}^* & \epsilon_{fy} &= C_E \epsilon_{fy}^* \\ f_{fu} &= C_E f_{fu}^* & \epsilon_{fu} &= C_E \epsilon_{fu}^* \end{aligned} \quad \text{Eq 1}$$

FRP Stress-Strain Relationship

A graphical representation of the FRP design strength curve is shown in Figure 3. E_{t1} and E_{t2} represent the initial and secondary moduli of elasticity values for the FRP system, respectively.

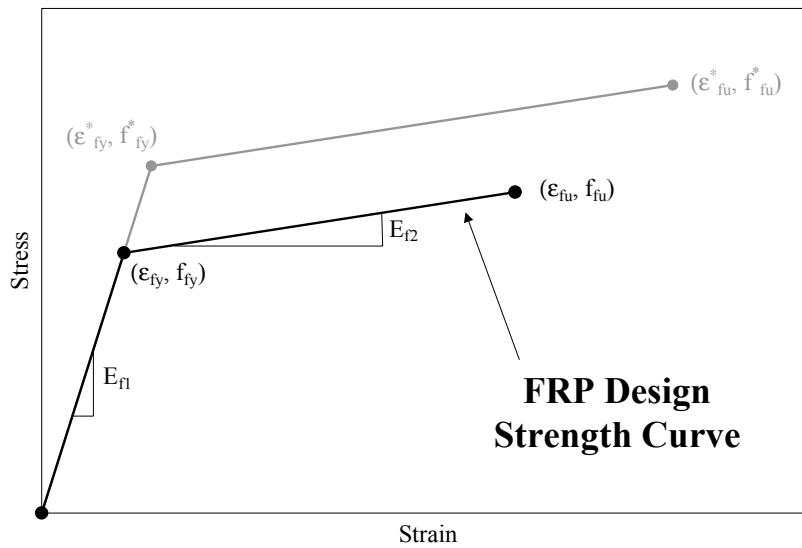


Figure 3. FRP design strength curve.

3 Load and Deformation Characteristics of FRP-Rehabilitated R/C Frames

Failure Modes

There are five failure modes that must be considered when determining the strength of an R/C member strengthened with FRP (GangRao and Vijay 1998):

1. Concrete crushing in compression prior to tension steel yielding
2. Concrete crushing in compression after tension steel yielding
3. Yielding of the steel followed by rupture of the FRP
4. FRP debonding from the concrete substrate
5. Concrete cover shear/tension failure (cover delamination).

The controlling failure mode can be determined by evaluating the strain levels in the concrete, steel, and FRP at section failure. FRP debonding, rupture of the FRP, or cover delamination can occur if the strain in the FRP reaches its flexural design rupture strain, $\kappa_m \epsilon_{fu}$, before the concrete reaches its maximum usable compressive strain, ϵ_{cu} . The bond-dependent coefficient for flexure, κ_m , limits the strain level in the FRP based on its stiffness. Calculating the strain in the tension steel at the ultimate load, ϵ_s , will determine if the steel has yielded. If $\epsilon_s < \epsilon_y$, the reliability and ductility of the member is low and the predicted strength is factored accordingly through the strength reduction factor, ϕ .

Flexural Capacity of Rehabilitated Frame Members

Assumptions

The calculated flexural capacity of R/C frame members strengthened with FRP is based on traditional R/C flexural behavior. Additional assumptions must be used, however, when FRP is bonded to the member. The following assumptions govern

the equations used to calculate the flexural capacity of R/C members strengthened with FRP:

1. Only the FRP bonded to the tension face of the member will be effective in resisting flexural loads.
2. The FRP reinforcement has a bilinear stress-strain relationship represented by the FRP design strength curve.
3. Perfect bond exists between the FRP reinforcement and concrete substrate.
4. The concrete strain at failure is 0.003.
5. The compressive strength of the concrete in flexure is $0.85f_c$.
6. The tensile strength of the concrete is ignored.
7. The steel reinforcement has an elastic-plastic stress-strain relationship.
8. Strains in the member are proportional to the distance from the neutral axis.

Note: The assumptions concerning the values of concrete stress and strain at failure and the use of an elastic-plastic stress-strain relationship should be used unless testing is performed that yields a more accurate representation of these parameters. The equations determining flexural capacity will have to be modified to take these changes into account.

The first assumption that only the FRP bonded to the tension face of the member will be effective in resisting flexural loads is based on research conducted by Al-Chaar (2000). Although FRP bonded to the sides and top of the beam are considered ineffective in flexure, it is still recommended to at least use a U-wrap to reduce the probability of FRP debonding, rupture of the FRP, cover delamination, and shear failure. A U-wrap is also more practical than fully wrapped because of the integral slabs present in most buildings. Figure 4 illustrates the FRP that should be considered effective when calculating the flexural capacity of a fully wrapped member and the recommended FRP wrapping scheme.

Using the assumptions for flexure, Figure 5 depicts the stress and strain distribution of a rectangular doubly reinforced concrete section strengthened with FRP at the ultimate load. The strain level in the concrete substrate at the time of FRP installation, ϵ_{bi} , must be considered when analyzing the section. This strain can be computed from an elastic analysis of the member under service loads.

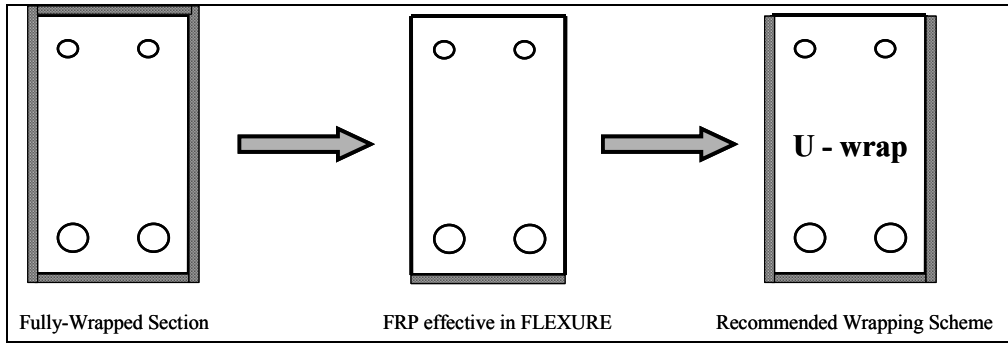


Figure 4. Effectiveness of FRP in flexure and the recommended FRP wrapping scheme.

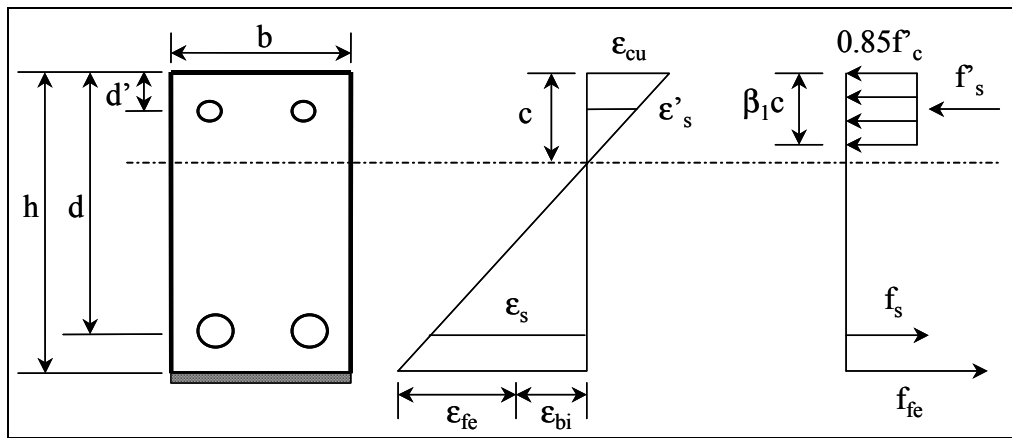


Figure 5. Stress and strain distribution at ultimate load.

Flexural Design

The governing design equation states that the design flexural capacity must equal or exceed the flexural demand (Eq 2). The flexural demand should be computed with the load factors recommended in ACI 318.

$$\phi M_n \geq M_{ult} \tag{Eq 2}$$

The nominal moment capacity for a rectangular doubly reinforced concrete member strengthened with FRP is given by Equation 3, where the moments of the internal beam forces are summed about the neutral axis.

$$M_n = A_s f_s (d - c) + A'_s f'_s (c - d') + \psi_f A_f f_{fe} (h - c) + 0.85 f'_c \beta_1 c b \left(1 - \frac{\beta_1}{2} \right) \tag{Eq 3}$$

The ratio of the depth of the equivalent rectangular stress block to the depth of the neutral axis, β_1 , is given by Equation 4 based on ACI 318.

$$0.85 \geq \beta_1 = 0.85 - 0.05(f'_c - 4 \text{ ksi}) \geq 0.65 \tag{Eq 4}$$

A reduction factor, ψ_f , should be applied to the flexural contribution of the FRP. This reduction factor is to account for the lower reliability of the FRP in comparison to steel. The reliability of the FRP is also a function of the wrapping scheme as shown in Table 3.

The effective strain in the FRP at failure, ε_{fe} , can be calculated using Equation 5. This equation assumes strain compatibility along with the inclusion of ε_{bi} . In addition, ε_{fe} is limited to the flexural design rupture strain, $\kappa_m \varepsilon_{fu}$, in order to reduce the probability that FRP debonding, rupture, or cover delamination might occur.

$$\varepsilon_{fe} = 0.003 \left(\frac{h-c}{c} \right) - \varepsilon_{bi} \leq \kappa_m \varepsilon_{fu} \quad \text{Eq 5}$$

The bond-dependent coefficient for flexure, κ_m , limits the strain level in the FRP based on the initial stiffness (E_{fi}), number of plies (n), and thickness (t) of the FRP. Equation 6 shows that κ_m has an inverse relationship with E_{fi} . In other words, the equation recognizes that FRP with a higher initial stiffness is more prone to delamination. This coefficient is based on recommendations from ACI 440. The bond-dependent coefficient is shown graphically in Figure 6.

$$0.9 \geq \kappa_m = \begin{cases} 1 - \frac{nE_{fi}t_f}{2400} & \text{for } nE_{fi}t_f \leq 1200 \\ \frac{600}{nE_{fi}t_f} & \text{for } nE_{fi}t_f \geq 1200 \end{cases} \quad \text{Eq 6}$$

Once the strain in the FRP is determined, the corresponding strains in the compression and tension reinforcing steel can be calculated from Equations 7 and 8.

$$\varepsilon'_s = (\varepsilon_{fe} + \varepsilon_{bi}) \left(\frac{c-d'}{h-c} \right) \quad \text{Eq 7}$$

$$\varepsilon_s = (\varepsilon_{fe} + \varepsilon_{bi}) \left(\frac{d-c}{h-c} \right) \quad \text{Eq 8}$$

Table 3. Values of ψ_f for flexural strengthening.

Wrapping Scheme	ψ_f
Fully-Wrapped	1.00
U-Wrap	0.95
Tension Face Only	0.85

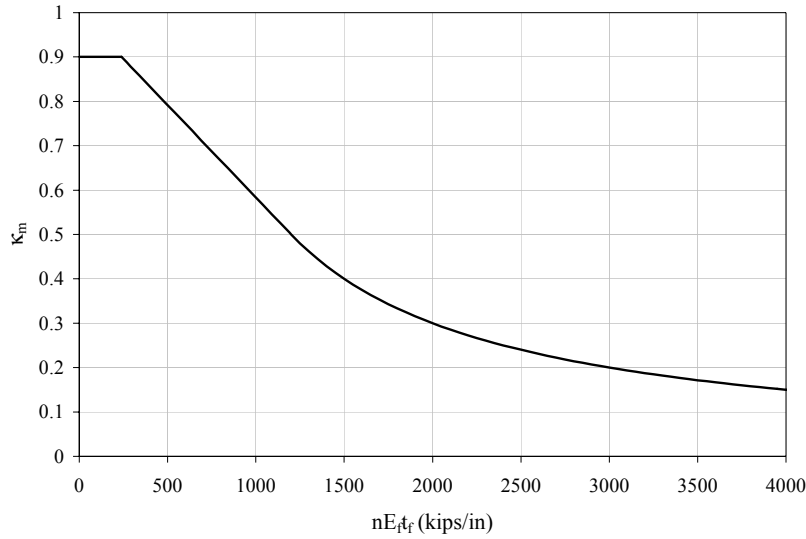


Figure 6. Bond-dependent coefficient, κ_m , for flexure.

The stress in the FRP depends on the level of strain. If the strain in the FRP is less than or equal to its yield strain, the FRP will behave linear elastically. Beyond the yield strain, the change in stress of the FRP corresponds to its secondary modulus. These two relationships are summarized in Equation 9.

$$f_{fe} = \begin{cases} E_{f1} \varepsilon_{fe} & \text{for } \varepsilon_{fe} \leq \varepsilon_{fy} \\ f_{fy} + E_{f2} (\varepsilon_{fe} - \varepsilon_{fy}) & \text{for } \varepsilon_{fe} > \varepsilon_{fy} \end{cases} \quad \text{Eq 9}$$

The stress in the compression and tension reinforcing steel can be found from Equations 10 and 11, which assume an elastic-plastic stress-strain relationship.

$$f'_s = \varepsilon'_s E_s \leq f_y \quad \text{Eq 10}$$

$$f_s = \varepsilon_s E_s \leq f_y \quad \text{Eq 11}$$

The depth to the neutral axis is determined by summing the internal beam forces to zero and maintaining strain compatibility. Equation 12 can be solved for c by an iterative process.

$$c = \frac{A_s f_s + A_f f_{fe} - A'_s f'_s}{0.85 f'_c \beta_1 b} \quad \text{Eq 12}$$

Finally, the nominal moment capacity must be multiplied by a strength reduction factor, ϕ , to account for the required reliability and ductility of the member. After

the application of FRP, the ductility of the member is often reduced. To account for this effect, the strength reduction factor is based on the strain level of the tension steel, ϵ_s , at the ultimate limit state according to Equation 13 and illustrated in Figure 7. The equations for ϕ are based on the guidelines in ACI 440.

$$\phi = \begin{cases} 0.90 & \text{for } \epsilon_s \geq 0.005 \\ 0.70 + \frac{0.20(\epsilon_s - \epsilon_y)}{0.005 - \epsilon_y} & \text{for } \epsilon_y < \epsilon_s < 0.005 \\ 0.70 & \text{for } \epsilon_s < \epsilon_y \end{cases} \quad \text{Eq 13}$$

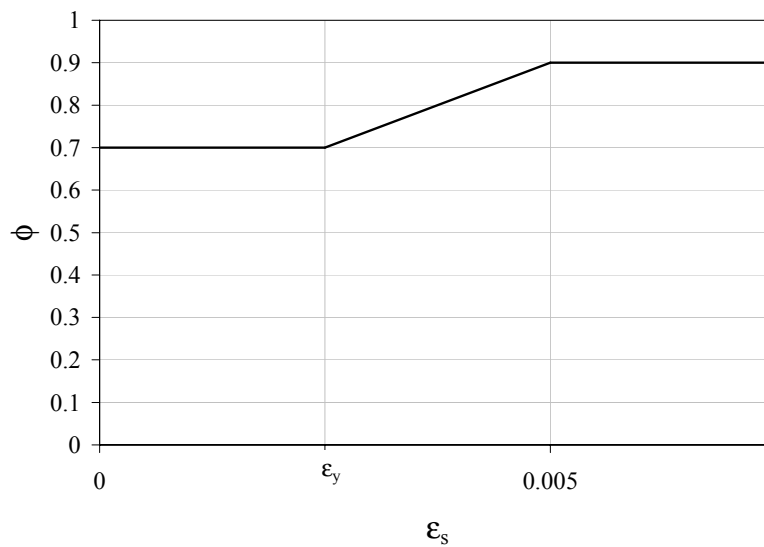


Figure 7. Strength reduction factor, ϕ .

Moment-Curvature Behavior of Rehabilitated Frame Members

The moment-curvature relationship for R/C members strengthened with FRP is dependent on many variables. In addition, the moment varies nonlinearly with the amount of curvature in the member. To simplify the calculations required to generate such a curve, a bilinear relationship as shown in Figure 8 is proposed.

The two points of the simplified curve are the yield and nominal flexural strength of the beam. The yield strength is defined as the smallest curvature that initiates yielding in either the reinforcing steel or FRP. For the case of the bottom steel reinforcement yielding first, the stress and strain distribution at M_y is shown in Figure 9.

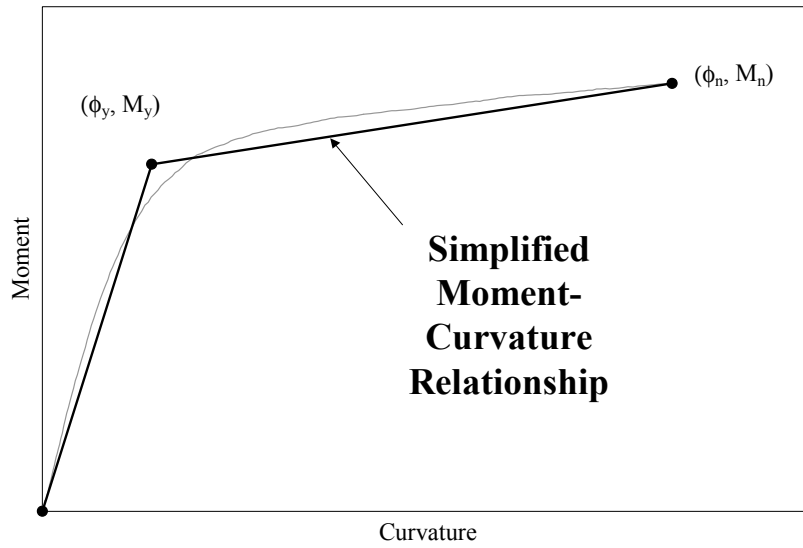


Figure 8. Simplified moment-curvature relationship.

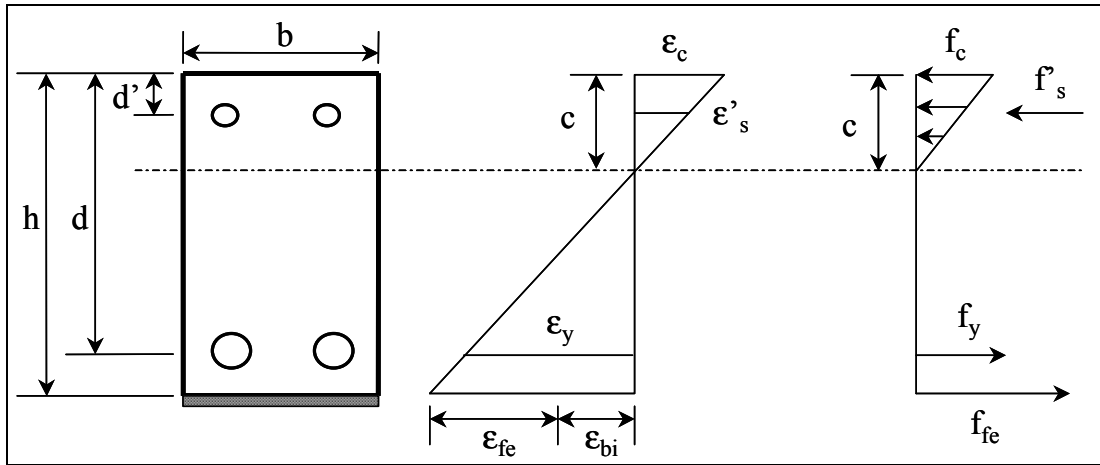


Figure 9. Stress-strain distribution at M_y .

Note that the stress distribution in the concrete is linearly proportional to the strain at this point. The yield strength of the member is determined by summing these forces about the neutral axis as shown in Equation 14. The nominal moment capacity is determined as before from Equation 3.

$$M_y = \begin{cases} \frac{bc^2}{3} f_c + A'_s f'_s (c - d') + A_s f_y (d - c) + \psi_f A_f f_{fe} (h - c) & \text{for } \epsilon_s = \epsilon_y, \epsilon_{fe} < \epsilon_{fy} \\ \frac{bc^2}{3} f_c + A'_s f'_s (c - d') + A_s f_s (d - c) + \psi_f A_f f_{fy} (h - c) & \text{for } \epsilon_{fe} = \epsilon_{fy}, \epsilon_s < \epsilon_y \end{cases} \quad \text{Eq 14}$$

The associated curvature at M_y and M_n is determined from Equations 15 and 16.

$$\phi_y = \frac{\varepsilon_y}{d - c} \quad \text{Eq 15}$$

$$\phi_n = \frac{\varepsilon_s}{d - c} \quad \text{Eq 16}$$

Shear Capacity of Rehabilitated Frame Members

The following procedure outlines the guidelines recommended by ACI 440 in order to determine the shear strength of R/C members strengthened with FRP. Providing adequate shear strength is crucial in promoting ductile flexural failure modes. The governing equation from ACI 318 states that the shear capacity must exceed the shear demand as shown in Equation 17.

$$\phi V_n \geq V_{ult} \quad \text{Eq 17}$$

The nominal shear strength is derived from three components: concrete, steel, and FRP. The FRP contribution is multiplied by an additional strength reduction factor as recommended by ACI 440. These relationships are illustrated in Equation 18.

$$V_n = V_c + V_s + \psi_f V_f \quad \text{Eq 18}$$

The values for ψ_f are dependent upon the wrapping scheme as shown in Table 4.

The different wrapping schemes are illustrated in Figure 10. Note that only the FRP bonded to the sides of the member are engaged in resisting shear. As in the recommendations for flexure, however, a U-wrap is the recommended FRP configuration.

Table 4. Values of ψ_f for shear strengthening.

Wrapping Scheme	ψ_f
Fully-Wrapped	0.95
U-Wrap or 2 sides	0.85

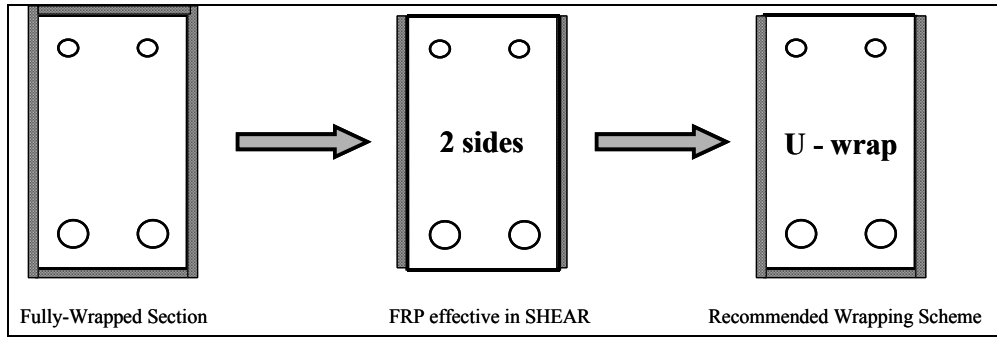


Figure 10. Effectiveness of FRP in shear and the recommended wrapping scheme.

The FRP contribution to shear resistance is dependent on the thickness, width, depth, spacing, and orientation of the FRP. The shear strength is given by Equation 19, while the area of FRP shear reinforcement is given by Equation 20. In addition, the variables affecting shear strength are illustrated in Figure 11.

$$V_f = \frac{A_{fv} f_{fe} (\sin \alpha + \cos \alpha) d_f}{s_f} \tag{Eq 19}$$

$$A_{fv} = 2nt_f w_f \tag{Eq 20}$$

The effective stress in the FRP is dependent on the effective strain and is found from Equation 21.

$$f_{fe} = \begin{cases} E_{f1} \epsilon_{fe} & \text{for } \epsilon_{fe} \leq \epsilon_{fy} \\ f_{fy} + E_{f2} (\epsilon_{fe} - \epsilon_{fy}) & \text{for } \epsilon_{fe} > \epsilon_{fy} \end{cases} \tag{Eq 21}$$

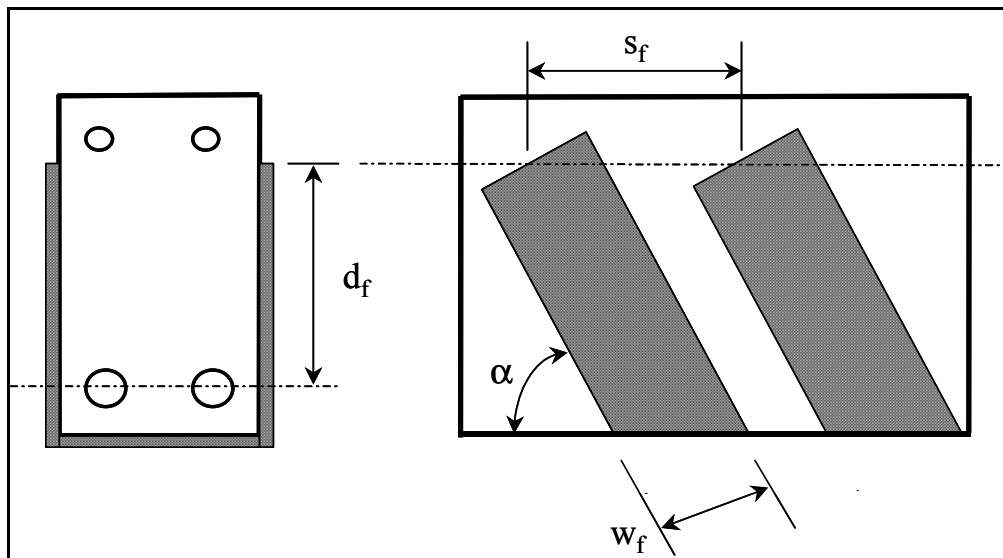


Figure 11. Variables used in shear strength calculations.

The effective strain utilized depends upon the wrapping scheme as shown in Equation 22. The strain limitation for the fully wrapped case is based on testing (Priestley et al. 1996). For U-wraps and FRP bonded on two sides only, delamination has been observed prior to loss of aggregate interlock. Therefore, bond stresses should be analyzed to determine an achievable effective strain level (Triantafillou 1998a,b,c).

$$\varepsilon_{fe} = \begin{cases} 0.004 \leq 0.75\varepsilon_{fu} & \text{Fully - Wrapped} \\ \kappa_v \varepsilon_{fu} \leq 0.004 & \text{U - Wraps or 2 sides} \end{cases} \quad \text{Eq 22}$$

The bond-dependent coefficient for shear, κ_v , is a function of the active bond length of the FRP laminate, the depth of the FRP strip, the effective strain level, the stiffness of the FRP, and the concrete strength. Equations 23 through 26 can be utilized to compute the bond-dependent coefficient (Khalifa et al. 1998).

$$\kappa_v = \frac{k_1 k_2 L_e}{468 \varepsilon_{fu}} \leq 0.75 \quad \text{Eq 23}$$

The active bond length is calculated using Equation 24.

$$L_e = \frac{2500}{(n t_f E_{f1})^{0.58}} \quad \text{Eq 24}$$

Two modification factors are used to determine the bond-dependent coefficient. These factors are a function of the concrete strength, the active bond length, and the depth of FRP shear reinforcement. Equations 25 and 26 are used to compute k_1 and k_2 .

$$k_1 = \left(\frac{f'_c}{4000} \right)^{\frac{2}{3}} \quad \text{Eq 25}$$

$$k_2 = \begin{cases} \frac{d_f - L_e}{d_f} & \text{for U - wraps} \\ \frac{d_f - 2L_e}{d_f} & \text{for 2 sides bonded} \end{cases} \quad \text{Eq 26}$$

Axial Compressive and Tensile Strength of Rehabilitated Frame Members

In traditional R/C design, steel stirrups provide the necessary confining pressure to support large axial loads. The same design ideology is used when analyzing R/C columns rehabilitated with FRP. The following assumptions govern the design equations for axial strength:

1. The FRP does not contribute directly to the compressive strength of the member.
2. The FRP fibers aligned transversely to the longitudinal axis of the column provide confining pressure, which increases the apparent compressive strength of the concrete.

Equation 27 gives the governing design equation for axial compression. The nominal axial load capacity of an R/C column strengthened with FRP is calculated from Equation 28. Note that the FRP does not contribute directly to the compressive strength. ACI 440 recommends using an additional strength reduction factor of $\psi_f = 0.95$.

$$\phi P_n \geq P_{ult} \quad \text{Eq 27}$$

$$P_n = 0.85\psi_f f'_{cc} (A_g - A_{st}) + f_y A_{st} \quad \text{Eq 28}$$

The term, f'_{cc} , is the confined concrete compressive strength and is calculated from Equation 29 (Mander et al. 1988).

$$f'_{cc} = f'_c \left[2.25 \sqrt{1 + 7.9 \frac{f_l}{f'_c}} - 2 \frac{f_l}{f'_c} - 1.25 \right] \quad \text{Eq 29}$$

The confining pressure due to the FRP jacket, f_l , is found from Equation 30.

$$f_l = \frac{\kappa_a \rho_f \varepsilon_{fe} E_{f1}}{2} \quad \text{Eq 30}$$

The effective strain in the FRP should be limited according to the guidelines in ACI 440 and Equation 31.

$$\varepsilon_{fe} = 0.004 \leq 0.75 \varepsilon_{fu} \quad \text{Eq 31}$$

The reinforcement ratio, ρ_f , and the efficiency factor, κ_a , for a circular section is given by Equations 32 and 33 where h refers to the diameter of the member and κ_a

is an efficiency factor for noncircular sections and, therefore, should be taken as unity. FRP confinement is the most efficient for circular members; therefore, the efficiency factor is set to unity.

$$\rho_f = \frac{4nt_f}{h} \quad \kappa_a = 1 \quad \text{Eq 32}$$

The reinforcement ratio for noncircular sections may be calculated using Equation 33.

$$\rho_f = \frac{2nt_f(b+h)}{bh} \quad \text{Eq 33}$$

The efficiency factor for noncircular sections is based on the geometry, aspect ratio, and configuration of steel reinforcement. This factor recognizes that non-circular members confined with FRP are not as efficient as circular ones and will always be less than unity. Equation 34 (Restrepo and DeVino 1996) should be used to calculate κ_a for aspect ratios (b/h) less than or equal to 1.5. For aspect ratios greater than 1.5, FRP has not proven to provide adequate confinement for increases in compressive strength.

$$\kappa_a = 1 - \frac{(b-2r)^2 + (h-2r)^2}{3bh(1-\rho_g)} \quad \text{for } \frac{b}{h} \leq 1.5 \quad \text{Eq 34}$$

The longitudinal reinforcement ratio, ρ_g , is calculated as the ratio of longitudinal steel area to the gross area of the member (Eq 35).

$$\rho_g = \frac{A_{st}}{A_g} \quad \text{Eq 35}$$

The variable r is defined as the radius of the edges of the section. This term is illustrated in Figure 12 and given by Equation 36.

$$r = \sqrt{\left(\frac{b}{2}\right)^2 + \left(\frac{h}{2}\right)^2} \quad \text{Eq 36}$$

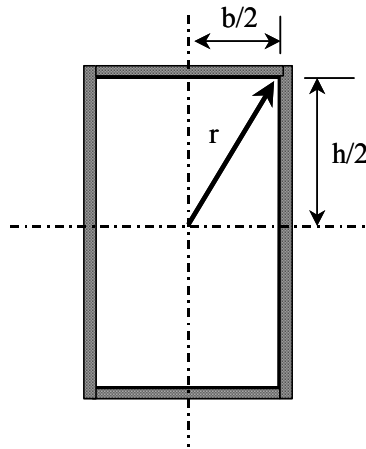


Figure 12. Illustration of the variable r .

The governing design equation for tensile strength is given by Equation 37. The tensile capacity of a member strengthened with FRP is directly related to the strain level. Therefore, the tensile strength can be found using Equation 38, where the additional FRP strength reduction factor is the same for axial compression.

$$\phi T_n \geq T_{ult} \quad \text{Eq 37}$$

$$T_n = \begin{cases} A_{st} f_y + \psi_f A_f E_{f1} \epsilon_{fe} & \text{for } \epsilon_{fe} \leq \epsilon_{fy} \\ A_{st} f_y + \psi_f A_f [f_{fy} + E_{f2} (\epsilon_{fe} - \epsilon_{fy})] & \text{for } \epsilon_{fe} > \epsilon_{fy} \end{cases} \quad \text{Eq 38}$$

The effective strain in the FRP can be determined based on the criteria given for shear strengthening given in Equations 23 through 26. Per ACI 440, the value of k_l in Equation 25 may be taken as unity, and a minimum bond length of $2L_e$ is recommended to develop this level of strain.

Moment-Thrust Interaction of Rehabilitated Frame Members

The moment-thrust interaction behavior of R/C members strengthened with FRP can be calculated using the equations presented thus far. The interaction curve is found by incrementing the depth to the neutral axis at ultimate load ($\epsilon_{cu} = 0.003$) and resolving the internal forces at each step. The axial force at each increment is the sum of the internal beam forces while the moment is found by summing the moment of these forces about the centerline of the section. Three points clearly define the moment-thrust envelope: P_n , M_n , and T_n . A typical interaction curve for an R/C column rehabilitated with FRP contrasted with a plain R/C column is shown in Figure 13.

Note that, slightly above the balanced failure condition (the rightmost point on the interaction curve), the curves for the bare column and the fully wrapped column merge. This is due to the assumption made earlier that only the FRP on the tension face of the member is effective in resisting flexural loads. In addition, another factor contributing to this phenomenon is that there are not any valid equations giving the desired transition from pure axial load to pure flexural load. If you recall, the equations for axial capacity were derived using confined concrete theory, while the equations for flexure rely on a direct stress-strain relationship to determine capacity. For any point on the interaction curve where $P > 0$ and $M > 0$, there is a combination of resistance due to concrete confinement and direct stress-strain relationships that is not clearly defined at this time.

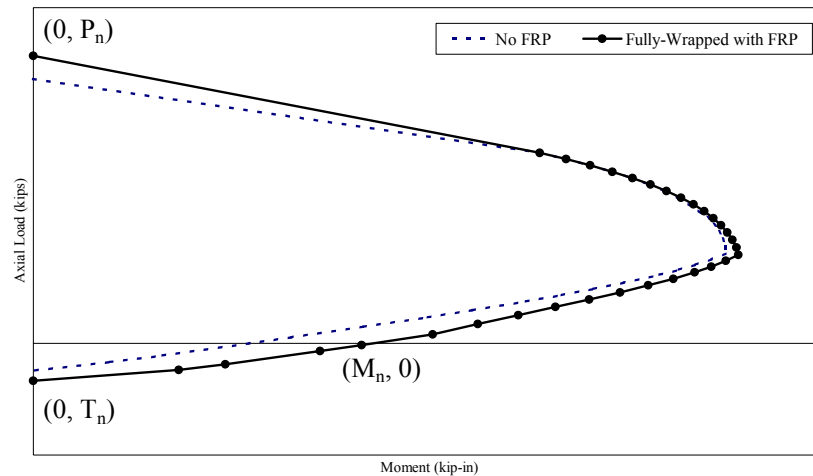


Figure 13. Moment-thrust interaction curve.

4 In-Plane Strength Evaluation of URM Infill Rehabilitated With FRP

Background

The transfer of lateral forces across rehabilitated infilled frames causes nonuniform stress distribution within the infill and frame elements. As the lateral forces are increased, the stress distribution varies until failure of the infill occurs. Failure of the infill occurs when either its shear or compressive strength is reached.

The expected flexural and shear strength of the frame elements confining the infill panel must also be evaluated. Column and beam shear and flexural strengths must exceed the horizontal/vertical components of the force required for failure of the infill. This procedure assures failure of the infill before failure in the confining frame occurs.

The lateral load capacity of rehabilitated frame-infill systems should be found using a nonlinear finite element program that captures the nonlinear behavior of all material components: masonry, mortar, concrete, steel, and FRP. Because this option is not available or is impractical in most situations, however, a simpler analytical method is proposed. The proposed method is a pushover analysis of a frame containing eccentric equivalent struts that represent the masonry. The method can be used for fully infilled frames as well as partially infilled and perforated masonry panels. Using eccentric struts in this global analysis will yield infill effects on the column directly, which will negate the need to evaluate these members locally. This method relies on the development of plastic hinges to capture the nonlinearities of the structural system. The proposed method has been proven to give reliable results based on experimental data and nonlinear finite element analysis. The following section gives a general outline of the process of performing a pushover analysis on an infilled frame rehabilitated with FRP.

General Evaluation Procedure Using Pushover Analyses

The following procedure is a general outline of what is required by standard structural analysis programs in order to perform a pushover analysis. More or less information may be required for a specific program. The methodology presented for evaluating the capacity of infilled frames rehabilitated with FRP is based on the ERDC/CERL report, *Evaluating Strength and Stiffness of Unreinforced Masonry Infill Structures* (Al-Chaar 2002). However, multiplicative factors have been added to account for the effects of the FRP.

1. Draw Frame Elements with the geometry, restraints, and material properties found in the existing structure. In general, the required material properties consist of f'_c , f'_y , E_c , and E_s . Definitions of these properties are given in the glossary.
2. Draw Equivalent Struts representing the infilled panels and place them eccentrically with respect to the columns. This eccentric distance is referred to as I_{column}^* . The strut thickness should be the same as the net thickness of the infill material it represents. The width of the equivalent strut, a , should be calculated according to the guidelines in this chapter. If the infilled panel is either partially infilled or perforated, the modifications in sections on partially infilled frames and perforated panels, respectively, must be applied. Furthermore, existing infill damage must be taken into account. Any rehabilitation performed on the masonry infill such as bonding FRP overlay to the infill surface should be taken into account as well. The material properties that should be assigned to the strut consist of R_{strut} and E_m , where R_{strut} is the capacity of the strut.
3. Assign Plastic Hinges to frame members with the load-deformation behavior appropriate for the particular structural section and material. For beams, the plastic hinge should identify nonlinear behavior for flexure and shear. Specifically, the flexural hinge should be based on the moment-curvature behavior for R/C members rehabilitated with FRP (Chapter 4). The shear hinge should be based on the capacity defined in Chapter 5. For columns, the hinge should account for the interaction between axial load and flexure as well as capture the nonlinearities associated with shearing. Chapter 6 can be used to obtain the moment-thrust envelope for the column. For plain R/C members, the hinge properties may be calculated using the guidelines given in Section 6.4 of FEMA 273. The

* Symbols referenced in this section are defined later in Chapters 7 and 8.

hinges in the columns should be located at a minimum distance l_{column} from the face of the beam, while hinges in the beam should be located at a minimum distance l_{beam} from the face of the column.

4. Assign Plastic Hinges to the midspan of the Eccentric Equivalent Struts with load-deformation characteristics consistent with Figure 24 (page 40).
5. Assign Rigid End Offsets (REOs) to the joints of the frame in order to represent the decreased flexibility of the frame members confined by infill. The REOs should extend from the joint outward along the beams and columns until a plastic hinge is intersected.
6. Apply the gravity loads as initial conditions of the pushover analysis. The load combinations recommended are those found in Equations 3-2 and 3-3 in FEMA 273. The lateral loads should be applied in a manner that approximates the inertia forces in the design earthquake. The recommended inertia force distributions are given in Section 3.3.3.2 of FEMA 273.
7. Perform the Pushover Analysis using any member-unloading method to obtain equilibrium after a plastic hinge loses capacity due to excessive deformation.

Using the general procedure outlined above, an engineer can reasonably predict the in-plane capacity of rehabilitated infilled frames. The following sections describe the evaluation process in more detail.

Equivalent Strut Width

In-plane strength predictions of infilled frames are a complex, statically indeterminate problem. The strength of a composite-infilled frame system is not simply the summation of the infill properties plus those of the frame. Great efforts have been invested, both analytically and experimentally, to better understand and estimate the composite behavior of masonry-infilled frames. Polyakov (1960) (work dating back to the early 1950s), Stafford-Smith (1962, 1966, 1969), Mainstone (1971), Klingner and Bertero (1976, 1978), to mention just a few, formed the basis for understanding and predicting infilled frame in-plane behavior. Their experimental testing of infilled frames under lateral loads resulted in specimen deformation shapes similar to the one illustrated in Figure 14.

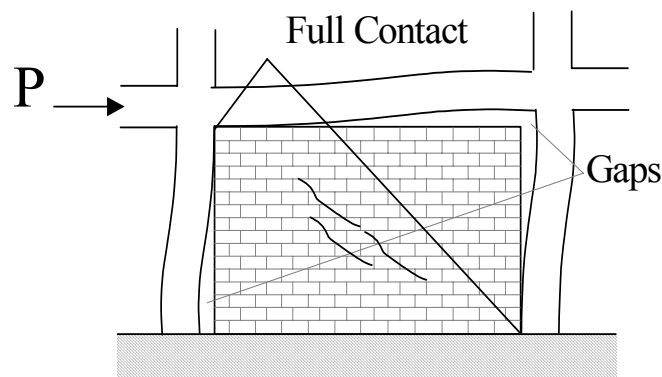


Figure 14. Specimen deformation shape.

During testing of the specimens, diagonal cracks developed in the center of the panel, and gaps formed between the frame and the infill in the nonloaded diagonal corners of the specimens, while full contact was observed in the two loaded diagonal corners. This behavior, initially observed by Polyakov, led to a simplification in infilled frame analysis by replacing the masonry infill with an equivalent compressive masonry strut as shown in Figure 15.

The equivalent masonry strut of width, a , with same net thickness and mechanical properties (such as the modulus of elasticity E_m) as the infill itself, is assumed to be pinned at both ends to the confining frame.

The evaluation of the equivalent width, a , varies from one reference to the other. The most simplistic approaches presented by Paulay and Priestley (1992) and Angel et al. (1994) have assumed constant values for the strut width, a , between 12.5 to 25 percent of the diagonal dimension of the infill, with no regard for any infill or frame properties. Stafford-Smith and Carter (1969), Mainstone (1971), and others, derived complex expressions to estimate the equivalent strut width, a , that consider parameters like the length of contact between the column/beam and the infill, as well as the relative stiffness of the infill to the frame.

The expressions used in this report have been adopted from Mainstone (1971) and Stafford-Smith and Carter (1969) for their consistently accurate predictions of infilled frame in-plane behavior when compared with experimental results (Mainstone 1971; Stafford-Smith and Carter 1969; Klingner and Bertero 1978; and Al-Chaar 1998). The masonry infill panel will be represented by an equivalent diagonal strut of width, a , and net thickness, t_{eff} , as shown in Figure 16.

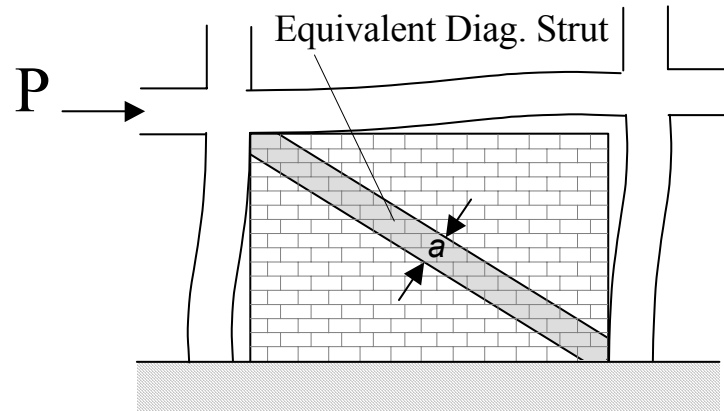


Figure 15. Equivalent diagonal strut.

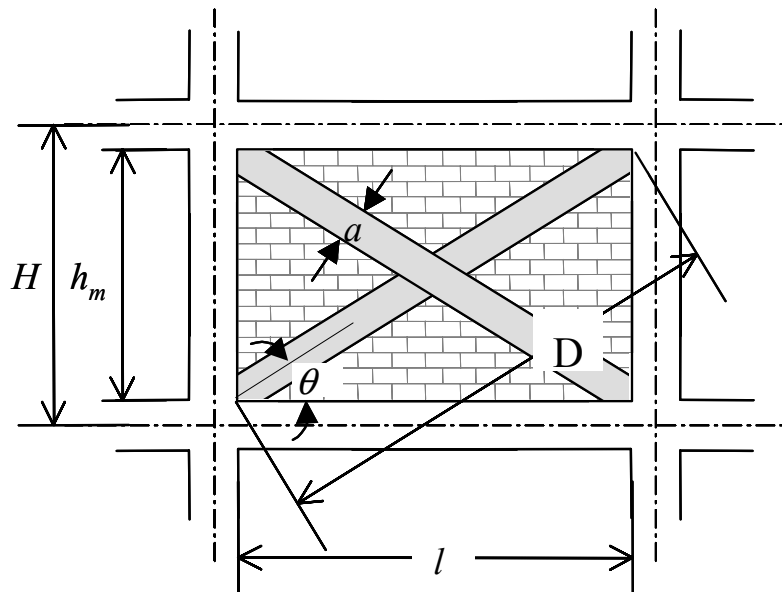


Figure 16. Strut geometry.

The equivalent strut width, a , depends on the relative flexural stiffness of the infill to that of the columns of the confining frame. The relative infill-to-frame stiffness shall be evaluated using Equation 39 (Stafford-Smith and Carter 1969):

$$\lambda_1 H = H \left[\frac{E_m t \sin 2\theta}{4E_c I_{col} h_m} \right]^{1/4} \quad \text{Eq 39}$$

Using this expression, Mainstone (1971) considers the relative infill-to-frame flexibility in the evaluation of the equivalent strut width of the panel as shown in Equation 40.

$$a = 0.175D(\lambda_1 H)^{-0.4} \quad \text{Eq 40}$$

If there are openings present, existing infill damage, and/or FRP overlay, however, the equivalent strut width must be modified using Equation 41.

$$a_{\text{mod}} = a(R_1)_i(R_2)_i\xi_i \quad \text{Eq 41}$$

Where:

$(R_1)_i$ = reduction factor for in-plane evaluation due to presence of openings (Eq 44).

$(R_2)_i$ = reduction factor for in-plane evaluation due to existing infill damage (Table 5, page 37).

ξ_i = strength increase factor due to presence of FRP overlay (Table 6, page 39).

Although the expression for equivalent strut width given by Equation 41 was derived to represent the elastic stiffness of an infill panel, this document will extend its use to determine the ultimate capacity of infilled structures. The strut will be assigned strength parameters consistent with the properties of the infill it represents. A nonlinear static procedure, commonly referred to as a pushover analysis, will be used to determine the capacity of the infilled structure.

Eccentricity of Equivalent Strut

The equivalent masonry strut is to be connected to the frame members as depicted in Figure 17, where the bold double-sided arrow represents the location of the strut in the structural model. The infill forces are assumed to be mainly resisted by the columns, and the struts are placed accordingly. The strut should be pin-connected to the column at a distance l_{column} from the face of the beam. This distance is defined in Equations 42 and 43 and is calculated using the strut width, a , without any reduction factors.

$$l_{\text{column}} = \frac{a}{\cos \theta_{\text{column}}} \quad \text{Eq 42}$$

$$\tan \theta_{\text{column}} = \frac{h_m - \frac{a}{\cos \theta_{\text{column}}}}{l} \quad \text{Eq 43}$$

Using this convention, the strut force is applied directly to the column at the edge of its equivalent strut width, a . Figure 17 illustrates this concept.

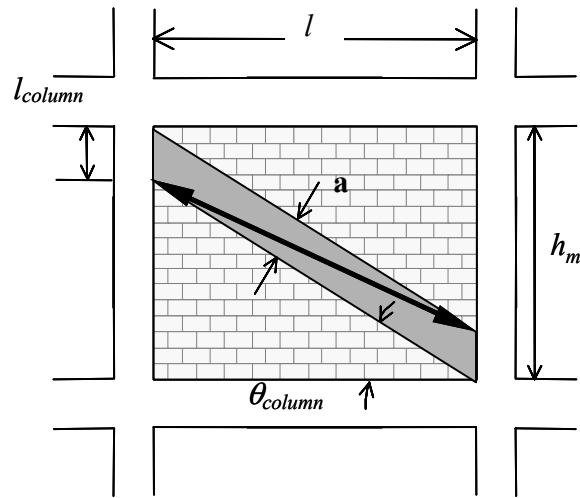


Figure 17. Placement of strut.

Partially Infilled Frames

In the case of a partially infilled frame, the reduced column length, l_{column} , is equal to the unbraced opening length for the windward column, while l_{column} for the leeward column is defined as usual (Figure 18). The strut width should be calculated from Equation 40, using the reduced infill height for h_m in Equation 39. Furthermore, the only reduction factor that should be taken into account is $(R_2)_i$, which accounts for existing infill damage.

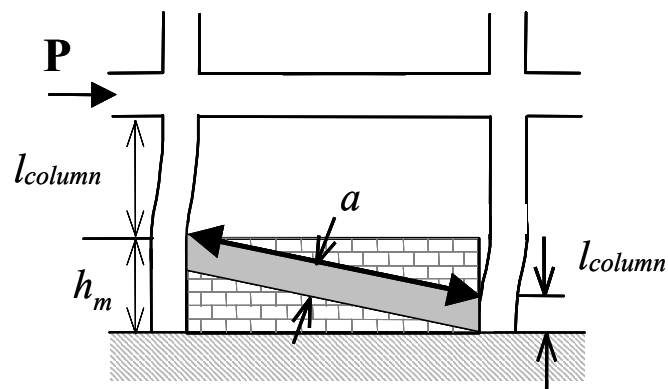


Figure 18. Partially infilled frame.

Perforated Panels

In the case of a perforated masonry panel, the equivalent strut is assumed to act in the same manner as for the fully infilled frame. Therefore, the eccentric strut should be placed at a distance l_{column} from the face of the beam as shown in Figure 19. The equivalent strut width, a , shall be multiplied, however, by a reduction

factor to account for the loss in strength due to the opening. The reduction factor, $(R_1)_i$, is calculated using Equation 44.

$$(R_1)_i = 0.6 \left(\frac{A_{open}}{A_{panel}} \right)^2 - 1.6 \left(\frac{A_{open}}{A_{panel}} \right) + 1 \quad \text{Eq 44}$$

Where:

A_{open} = area of the openings (in.²)

A_{panel} = area of the infill panel (in.²) = $l \times h_m$

Note: If the area of the openings (A_{open}) is greater than or equal to 60 percent of the area of the infill panel (A_{panel}), then the effect of the infill should be neglected, i.e., $(R_1)_i = 0$.

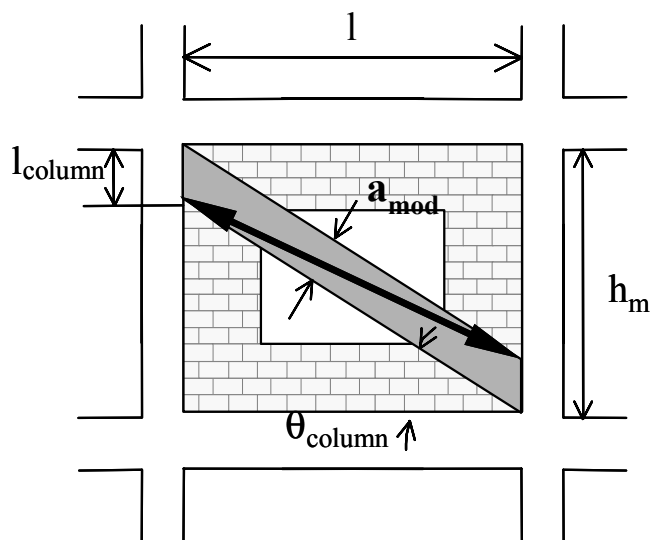


Figure 19. Perforated panel.

Note that reducing the strut width to account for an opening does not necessarily represent the stress distributions likely to occur. This method is a simplification in order to compute the global structural capacity. Local effects due to an opening should be considered by either modeling the perforated panel with finite elements or using struts to accurately represent possible stress fields as shown in Figure 20.

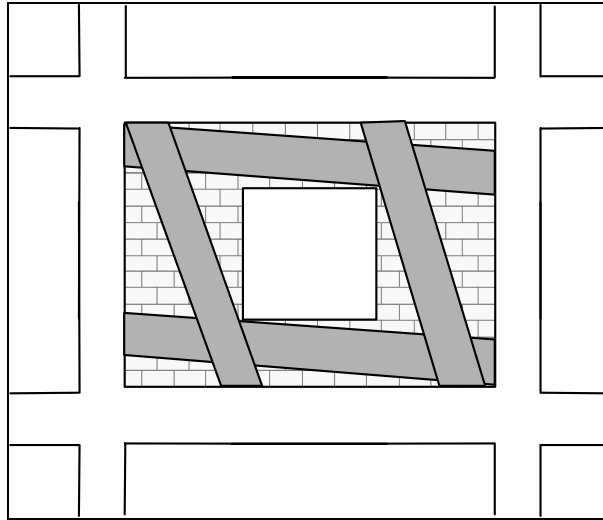


Figure 20. Possible strut placement for perforated panel.

Existing Infill Damage

Masonry infill panel behavior deteriorates as the elastic limit is exceeded. For this reason, it is important to determine whether the masonry in the panel has exceeded the elastic limit and, if so, by how much. The extent of existing infill damage can be determined by visual inspection of the infill. Existing panel damage (or cracking) must be classified as either: no damage, moderate damage, or severe damage as presented in Figure 21. If in doubt as to the magnitude of existing panel damage, assume severe damage for a safer (conservative) estimate. A reduction factor for existing panel damage $(R_2)_i$ must be obtained from Table 5. Note that, if the slenderness ratio (h_m/t) of the panel is greater than 21, $(R_2)_i$ is not defined and repair is required. For panels with no existing panel damage, the reduction factor $(R_2)_i$ must be taken as 1.0.

Table 5. In-plane damage reduction factor.

h_m/t	$(R_2)_i$ for Type of Damage	
	Moderate	Severe
≤ 21	0.7	0.4
> 21	Requires Repair	

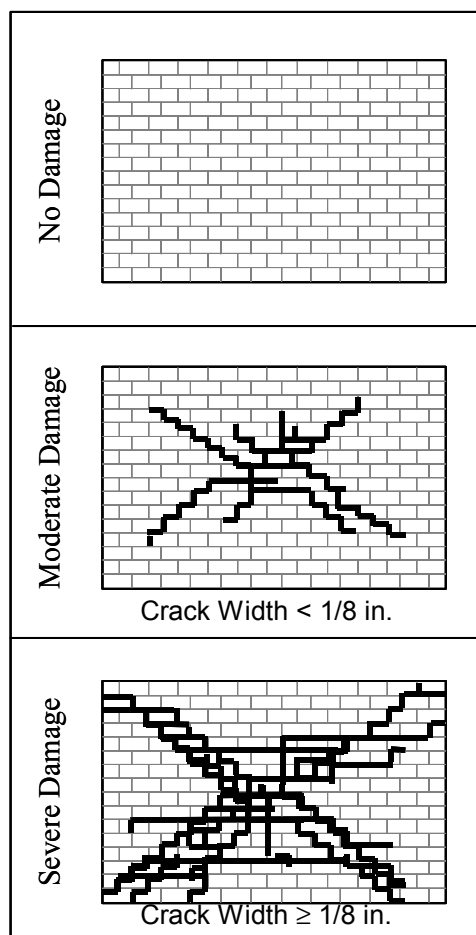


Figure 21. Visual damage classification.

Infill Rehabilitated With FRP

When FRP is bonded to the surface of masonry infill, the strength of the composite section increases. Figure 22 shows several different bonding schemes used to strengthen masonry walls.

Depending on the FRP strip orientation and the number of layers used, a different strength increase factor for FRP must be utilized. Based on research performed by ERDC, a table of FRP strength increase factors, ξ_l , was developed (Table 6). These factors were developed from testing of URM panels, with fairly uniform aspect ratios. The picture frame and reinforced picture frame FRP strip orientations did not yield reliable increases in strength and, therefore, ξ_l for these cases should be taken as unity.

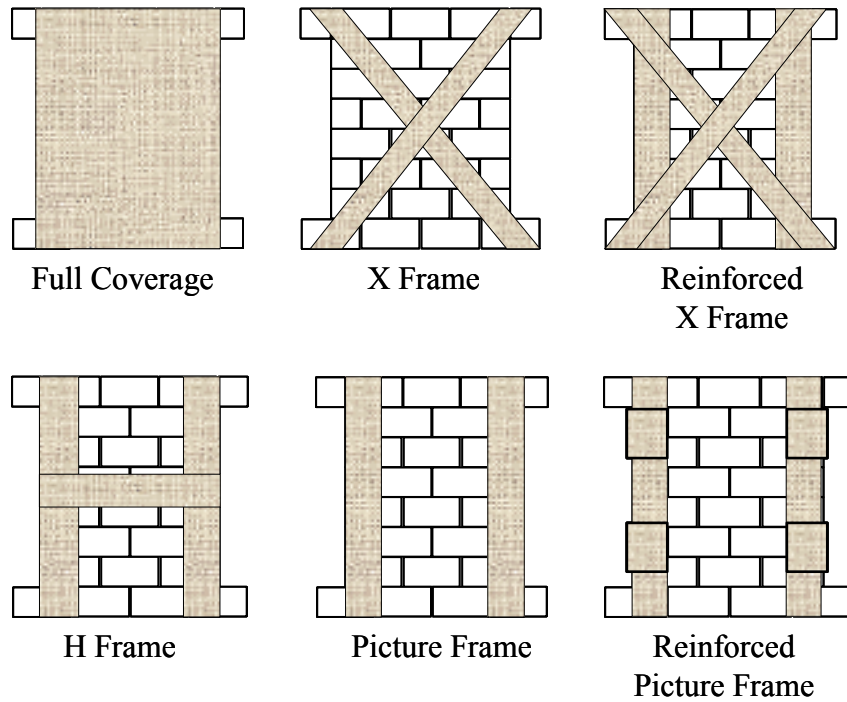


Figure 22. FRP strip orientation used on masonry walls.

Table 6. FRP strength increase factors.

FRP Strip Orientation	ξ_1
2 Layer Full Coverage	1.51
1 Layer Reinforced X Frame	1.48
1 Layer Full Coverage	1.41
2 Layer X Frame	1.33
1 Layer X Frame	1.29
1 Layer H Frame	1.20

Load-Deformation Behavior of the Eccentric Equivalent Strut

The eccentric equivalent strut used to model the masonry infill is pin-connected to the frame elements so that no moment transfer occurs. The strength of the strut is determined by calculating the load required to reach masonry infill crushing strength (R_{cr}) (Equation 47) and the load required to reach the masonry infill shear strength (R_{shear}) (Equation 48). The component of these forces in the direction of the equivalent strut will be used to assign the strut a “compressive” strength. This strength is defined as R_{strut} (Equation 45) and governs the strength of the plastic hinge in the strut:

$$R_{strut} = \min \left\{ \begin{array}{l} R_{cr} \\ R_{shear} / \cos \theta_{strut} \end{array} \right\} \quad \text{Eq 45}$$

$$\tan \theta_{strut} = \frac{h_m - 2l_{column}}{l} \quad \text{Eq 46}$$

where:

θ_{strut} = the angle of the eccentric strut with respect to the horizontal, given by Equation 46 and shown in Figure 23. The equivalent strut is assumed to deflect to nonlinear drifts, as Figure 24 illustrates.

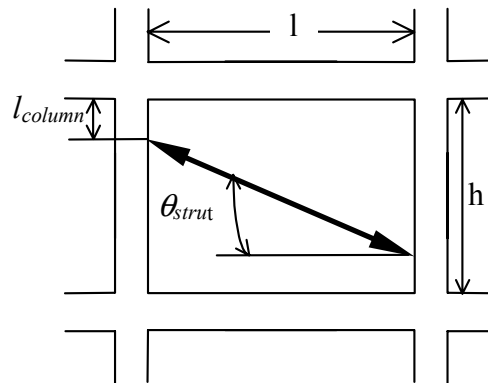


Figure 23. Geometry of θ_{strut} .

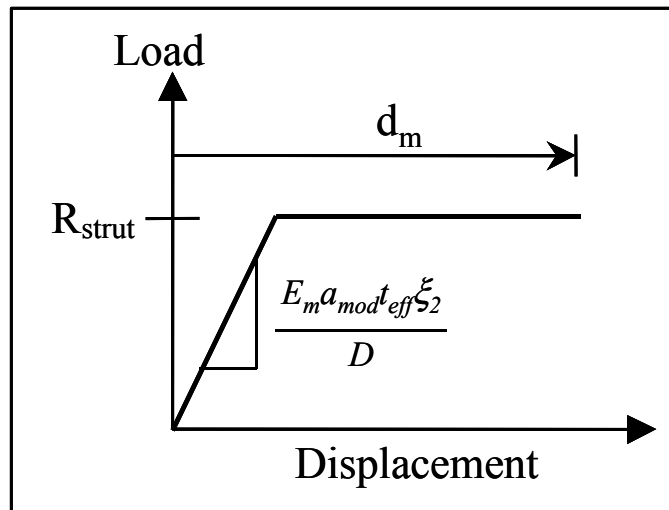


Figure 24. Load-deformation behavior.

The parameter, d_m , which represents the nonlinear lateral drift associated with the infilled panel, is defined in Table 7-7 of FEMA 273. The stiffness of the strut will be governed by the modulus of elasticity of the masonry material (E_m), the cross-sectional area ($a_{mod} \times t_{eff}$), and the presence of any FRP. The variable, ξ_2 , is a stiffness increase factor for FRP based on research performed by ERDC. Table 7 gives different stiffness increase factors depending on the FRP pattern. Recall the FRP patterns illustrated in Figure 22.

Table 7. FRP stiffness increase factors.

FRP Pattern	ξ_2
Full Coverage	1.53
Reinforced X-frame	1.43
Reinforced Picture Frame	1.39
H-frame	1.27
X-frame	1.23
Picture Frame	1.16

Masonry infill crushing strength

The masonry infill crushing strength corresponds to the compressive load that the equivalent masonry strut can carry before the masonry is crushed (R_{cr}). The applied load that corresponds to the crushing strength of the infill is evaluated using Equation 47.

$$R_{cr} = a_{\text{mod}} t_{\text{eff}} f'_m \quad \text{Eq 47}$$

where:

f'_m = compressive strength of the masonry (ksi)

t_{eff} = net thickness of the masonry panel (in.)

Masonry infill shear strength

The shear capacity of masonry is provided by the combination of two different mechanisms: the bond shear strength and the friction between the masonry and the mortar. The concept of the bond shear strength is illustrated in Figure 25, where a typical stair-stepped shear crack is approximated by a single shear crack through a bed joint. This simplification is valid because the vertical component of the stair-stepped crack will be in tension, and its contribution to the shear strength should be neglected. Therefore, the horizontal lateral load required to reach the infill shear strength is calculated by Equation 48.

$$R_{\text{shear}} = A_n f'_v (R_1)_i (R_2)_i \xi_1 \quad \text{Eq 48}$$

where:

A_n = net cross sectional mortar/grouted area of infill panel along its length (sq in.)
 $= t_{\text{eff}} * l$

f'_v = masonry shear strength (ksi)

Note: Although vertical loads on infills may not be accurately estimated, 20 percent of the normal stress may be assumed to be resisted by the infill and included in the friction component of the resisting mechanism.

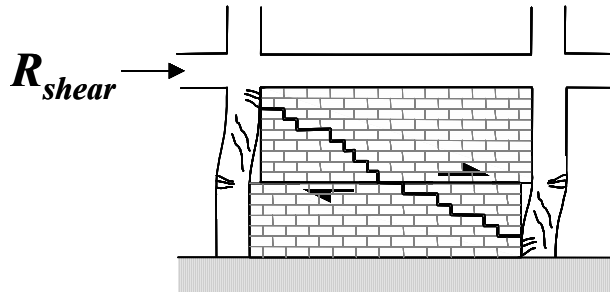


Figure 25. Shear failure of masonry.

Plastic Hinge Placement

Plastic hinges in columns should capture the interaction between axial load and moment capacity. These hinges should be located at a minimum distance l_{column} from the face of the beam. Hinges in beams need only characterize the flexural behavior of the member. These hinges should be placed at a minimum distance l_{beam} from the face of the column. This distance is calculated from Equations 49 and 50 where θ_{beam} is the angle at which the infill forces would act if the eccentricity of the equivalent strut was assumed to act on the beam as depicted in Figure 26.

$$l_{beam} = \frac{a}{\sin \theta_{beam}} \quad \text{Eq 49}$$

$$\tan \theta_{beam} = \frac{h_m}{l - \frac{a}{\sin \theta_{beam}}} \quad \text{Eq 50}$$

Although the infill forces are assumed to act directly on the columns, hinging in the beams will still occur and l_{beam} is a reasonable estimate of the distance from the face of the column to the plastic hinge.

Shear hinges must also be incorporated in both columns and beams. The equivalent strut, however, only needs hinges that represent the axial load. This hinge should be placed at the midspan of the member. In general, the minimum number and type of plastic hinges needed to capture the inelastic actions of an infilled frame are depicted in Figure 27.

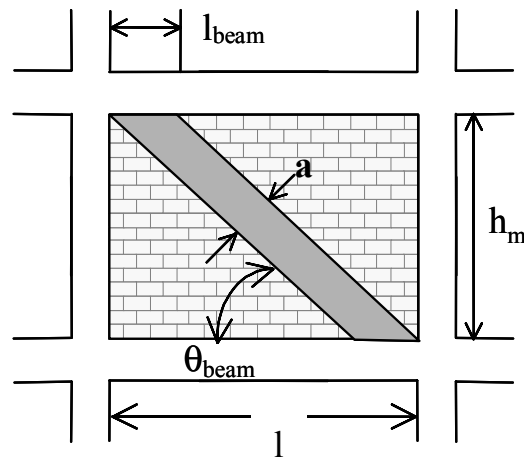


Figure 26. Distance to beam hinge.

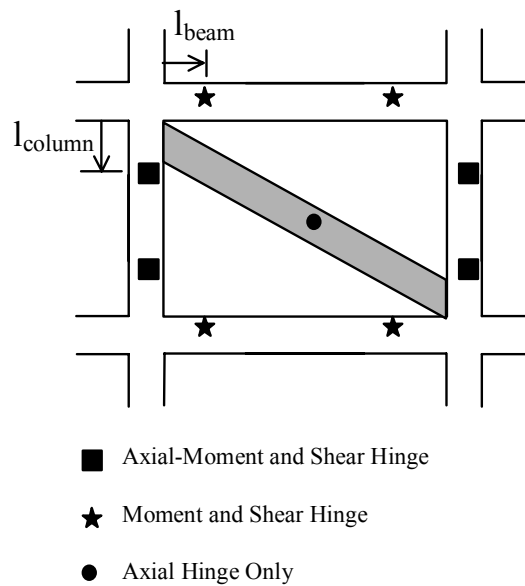


Figure 27. Plastic hinge placement.

Although lateral loading generally leads to hinge formation near the end of a member, inelastic deformation may occur at other locations, especially when large gravity loads are present. Therefore, the possibility of hinging near midspan must not be overlooked. In addition, the engineer is allowed to place hinges differently if the placement is justified and good engineering judgment is used.

Rigid End Offsets

The frame elements surrounding a panel containing an equivalent strut in the mathematical model described thus far will be more flexible than the actual structure. This is due to the lack of confinement provided by the strut to the frame elements relative to an infilled frame. To counteract this effect, it is recommended that REOs be placed on the frame members surrounding an infilled panel. For beams surrounding infilled panels, REOs should be used from the beam/column joint to a distance of l_{beam} from the face of the column. For columns surrounding infilled panels, REOs should be placed from the beam/column joint to a distance of l_{column} from the face of the beam. These distances also correspond to the locations of the beam and column plastic hinges. The beam or column is therefore assumed to be rigid up to the point of the plastic hinge. Figure 28 shows the placement of REOs (shown in black) for an infilled frame.

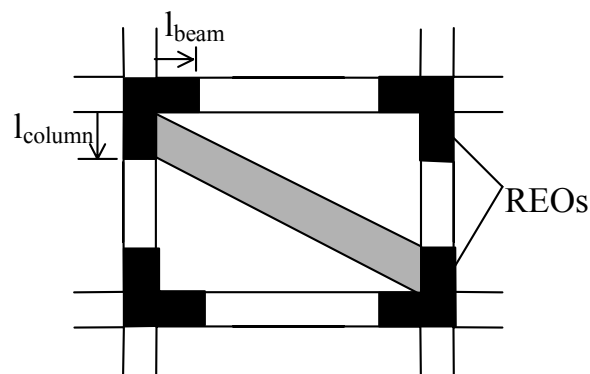


Figure 28. Rigid end offset placement.

Loading

The mathematical model should be subjected to monotonically increasing lateral loads until the maximum displacement of the design earthquake is reached or a failure mechanism forms. The target displacement should be calculated following the procedure in Section 3.3.3.3 of FEMA 273. Gravity loads should be applied as initial conditions prior to the earthquake loadings. The load combinations that should be used are given by Equations 3-2 and 3-3 in FEMA 273.

Lateral loads should be applied in a manner that approximates the inertia forces in the design earthquake. It is recommended that a minimum of two different inertia force distributions be used in order to capture the worst-case design forces. The recommended inertia force distributions are given in Section 3.3.3.2 of FEMA 273.

5 In-Plane Stiffness Evaluation of URM Infill Rehabilitated With FRP

The following procedure should be used to resolve the stiffness of structures containing fully infilled panels, partially infilled panels, and/or perforated masonry panels rehabilitated with FRP. This method relies on exploiting the pushover curve generated by the structural analysis program for capacity evaluation. The pushover curve must be modified, however, to accurately represent displacements. Modifications must be made in order to increase the initial stiffness and reduce the displacement at ultimate load since the use of an equivalent strut in the pushover analysis yields mathematical models, which are more flexible than experimental models.

The general procedure for correcting the pushover curve consists of approximating the curve with a bilinear load-deflection relationship. The slopes of both segments of the bilinear curve are then increased while keeping the yield and ultimate loads constant. In effect, the values for initial stiffness and displacement at ultimate are modified to more reasonable values.

Bilinear Load-Deflection Behavior

The bilinear load-deflection curve is defined by three points: the origin, the yield load and displacement (V_y and Δ_y), and the ultimate load and displacement (V_u and Δ_u). The yield load, as used within this report, does not refer to any specific material yielding, but only to signify a change in stiffness represented by the bilinear load-deflection curve. The bilinear curve is also defined by two stiffnesses, K_y and K_u , which are the slopes of the initial and final portions of the curve. The bilinear curve should be drawn in a manner that minimizes the deviations from the actual pushover curve as shown in Figure 29.

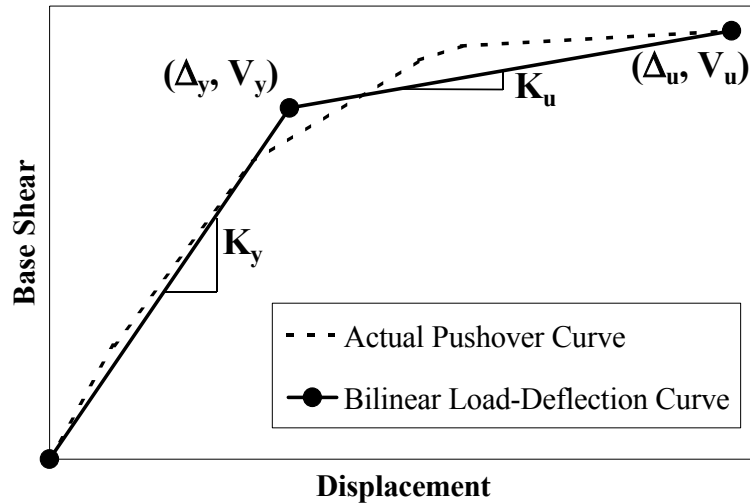


Figure 29. Bilinear load-deflection curve.

Once the bilinear curve has been drawn, it must be modified to increase the initial stiffness and decrease the displacement at ultimate load to more reasonable values. The yield and ultimate loads are held constant while K_y and K_u are increased to K_i and K_f , respectively. K_i represents the actual initial elastic stiffness of the infilled structure, while K_f represents the final stiffness (i.e., the stiffness from the yield load to the ultimate load). Figure 30 shows the modified bilinear load-deflection curve. Δ_y' represents the modified displacement at yield, while Δ_u' represents the actual displacement of the infilled structure at ultimate load.

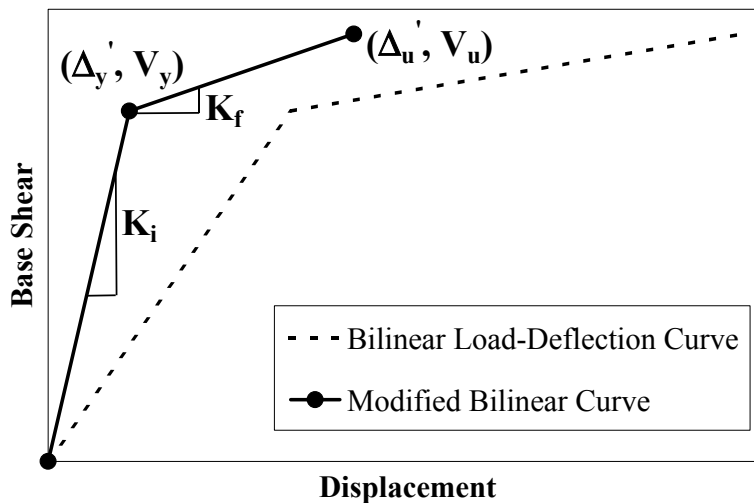


Figure 30. Modified load-deflection curve.

The modified bilinear curve better represents the initial stiffness and displacement at ultimate load for the infilled structure. The procedure for determining K_i and K_f , as well as the rationale for such modifications, is discussed in the following section.

Determination of K_i and K_f

The pushover curve of a masonry-infilled structure that is modeled with eccentric equivalent struts and used to determine the *capacity* will result in stiffnesses that are too low relative to experimental results. The initial stiffness is too small and the displacement at ultimate is too large. These results stem from the approximation when using an equivalent strut to represent a masonry-infilled panel.

The equation used to calculate the equivalent strut width for determining the capacity of the infill panel is based on a more conservative approach by Mainstone (1971), which establishes a lower bound of the expected elastic stiffness of the infill (shown by the lower curve in Figure 31). Mainstone (1971) only considered the relative infill-to-frame flexibility in the evaluation of the equivalent strut width of the panel. Upper bound estimates for elastic stiffness, according to Stafford-Smith and Carter (1969), vary not only with the relative infill-to-frame stiffness but also with the aspect ratio of the panel (l/h_m) as illustrated in Figure 31 (for $l/h_m = 1.0, 1.5, 2.0,$ and 2.5). The largest possible values for a/D correspond to panels with aspect ratios (l/h_m) of 1.0. For l/h_m ratios smaller than 1.0, the inverse of the ratio should be used to determine the equivalent strut width.

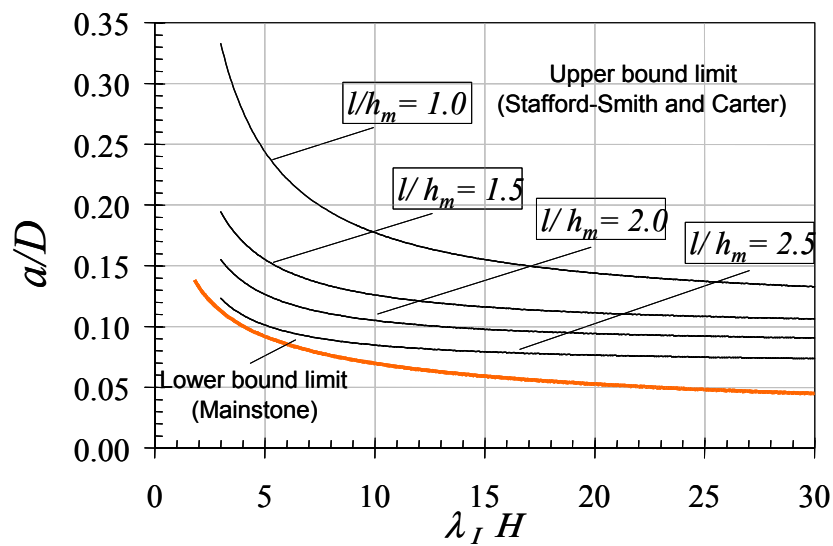


Figure 31. Upper / lower limit strut width.

Equivalent strut width estimates by Stafford-Smith and Carter (1969) may also be obtained using Equations 51 and 52, for panels with panel aspect ratios greater than or equal to 1.5. For aspect ratios of 1.0, Equation 53 must be used. Linear interpolation is allowed for panel aspect ratios between 1.0 and 1.5.

$$a = 0.0835CD \left(1 + \frac{2.574}{\lambda_y H} \right) \text{ for } l/h_m \geq 1.5 \quad \text{Eq 51}$$

$$C = -0.3905 \left(\frac{l}{h} \right) + 1.7829 \quad \text{Eq 52}$$

$$a = 0.1106D \left(1 + \frac{6.027}{\lambda_y H} \right) \text{ for } l/h_m = 1.0 \quad \text{Eq 53}$$

From Figure 31, for aspect ratios between 1.0 and 1.5, Mainstone (1971) underestimates the strut width, a , by a significant amount. As the aspect ratio increases past 1.5, the difference in strut width estimates between Mainstone (1971) and Stafford-Smith and Carter (1969) decreases. Therefore, the initial bilinear stiffness, K_y , found from the pushover analysis and based on equations from Mainstone (1971), must be corrected to account for the inadequate stiffness provided by the strut calculated from Equation 40. The following two methods are proposed to increase the initial stiffness.

The first method increases the existing K_y by a factor of three, but is applicable only for infill panels with an aspect ratio between 0.67 and 1.5. This assumption allows the engineer to use the existing data obtained from the pushover analysis and avoid creating another mathematical model. The factor of three accounts for the difference in strut width estimates found by Mainstone (1971) compared to Stafford-Smith and Carter (1969). **Note:** This method is only an approximation. It is suggested to verify the calculated stiffness by following the second procedure discussed next.

The second method can be used for any aspect ratio, but *must* be used for aspect ratios less than 0.67 or greater than 1.5. This method uses the equations by Stafford-Smith and Carter (1969) to calculate a strut width (Eq 51-53). Using these strut widths, a new mathematical model must be constructed and the elastic stiffness of this model should be used as the initial elastic stiffness of the infilled structure. This stiffness is referred to as K_{SSC} and represents the initial elastic stiffness determined by Stafford-Smith and Carter (1969). The two methods are summarized in Equation 54.

$$K_i = \begin{cases} 3K_y & (0.67 \leq \frac{l}{h} \leq 1.5) \\ K_{SSC} & (\text{any } \frac{l}{h}) \end{cases} \quad \text{Eq 54}$$

The final stiffness must also be increased in order to reduce the displacement at ultimate load to more reasonable values. Increasing the secondary stiffness from the pushover K_u by a factor of two along with increasing the initial stiffness to K_i and keeping the yield and ultimate loads constant led to displacement at ultimate load, which matched experimental values fairly well. The relationship for K_f is expressed in Equation 55.

$$K_f = 2K_u \quad \text{Eq 55}$$

Using the calculated values for K_i and K_f , the modified bilinear load-deflection relationship should reasonably predict the initial stiffness (K), ultimate load capacity (V_u), and displacement at ultimate load (Δ_u) of the infilled structure.

6 Summary

This project presented guidelines for evaluating strength and stiffness of unreinforced masonry (URM) infill panels rehabilitated with FRP and subjected to lateral forces. Based on experimental and computational research performed at ERDC, the guidelines include a number of empirically based relationships for estimating strength and stiffness of infill panels subjected to lateral forces. The guidelines give the engineer a strength-based alternative to FEMA 273 (a performance-based method), which should also result in safe and economical construction.

The information compiled in this report was written following a logical sequence intended to help the engineer in the structural evaluation process. First, it outlined the steps that must be followed to obtain all the required material and geometrical properties of the structure to be evaluated. The next chapters presented the load and deformation characteristics of R/C members strengthened with FRP. Next, the in-plane strength and stiffness evaluation procedures were shown for the lateral-force resisting system consisting of infilled frames rehabilitated with FRP.

The evaluation procedures presented in this report (based on life-safety performance) are applicable to all building structures that have been constructed with R/C frames and walls that consist of infill panels constructed of solid clay brick, concrete block, and hollow clay tile masonry. These types of structures correspond to Building type 10 as defined in Chapter 2 and in accordance with FEMA 310.

References

Cited

- ACI Committee 318, "Building Code Requirements for Structural Concrete," American Concrete Institute (ACI), Detroit, MI, 1995.
- ACI Committee 440, "Guide for the Design and Construction of Externally Bonded FRP Systems for Strengthening Concrete Structures," ACI, Detroit, MI, October 2001.
- Al-Chaar, G., 2000, "Seismic Rehabilitation of Existing Reinforced Concrete and Masonry Structures Using Composite Overlay Materials," *Scientific Research Outlook*, University of Sharjah, United Arab Emirates, April 2000.
- Al-Chaar, G., 2002, *Evaluating Strength and Stiffness of Unreinforced Masonry Infill Structures*, U.S. Army Engineer Research and Development Center, Construction Engineering Research Laboratory (ERDC/CERL) TR-02-1/ADA407072, January 2002.
- Al-Chaar, G., 1998, *Non-Ductile Behavior of Reinforced Concrete Frames with Masonry Infill Panels Subjected to In-Plane Loading*, ERDC/CERL Technical Manuscript 99/18/ADA360129, December 1998.
- Angel, R., D.P. Abram, D. Shapiro, J. Uzarski, and M. Webster, 1994, *Behavior of Reinforced Concrete Frames with Masonry Infills*, Structural Research Series No. 589, UILU-ENG-94-2005, University of Illinois at Urbana, March 1994.
- Federal Emergency Management Agency (FEMA) 273, *NEHRP Guidelines for the Seismic Rehabilitation of Buildings*, October 1997.
- FEMA 310, *Handbook for the Seismic Evaluation of Buildings – A Prestandard*, January 1998.
- GangRao, H.V.S. and P.V. Vijay, 1998, "Bending Behavior of Concrete Beams Wrapped with Carbon Fabric," *Journal of Structural Engineering*, No. 124, pp 3-10.
- Khalifa, A., W. Gold, A. Nanni, and M. Abel-Aziz, 1998, "Contribution of Externally Bonded FRP to the Shear Capacity of RC Flexural Members," *Journal of Composites in Construction*, V. 2, No. 4, November 1998.
- Klingner, R.E. and V. Bertero, 1976, *Infilled Frames in Earthquake-Resistant Construction*, Report No. EERC 76-32, Earthquake Engineering Research Center, University of California, Berkeley, December 1976.
- Klingner, R.E. and V. Bertero, 1978, "Earthquake Resistance of Infilled Frames," *Journal of the Structural Division*, American Society of Civil Engineers (ASCE), Vol. 104, June 1978.

- Mainstone, R. J., 1971, "On the Stiffness and Strength of Infilled Frames," *Proceedings of the Institution of Civil Engineers*.
- Mander, J.B., M.J.N. Priestley, and R. Park, 1988, "Theoretical Stress-Strain Model for Confined Concrete," *Journal of Structural Engineering*, ASCE, Vol. 114, No. 8, pp 1804-1826.
- Paulay, T. and M.J.N. Priestley, 1992, *Seismic Design of Reinforced Concrete and Masonry Buildings*, John Wiley & Sons.
- Priestley, M., F. Seible, and G. Calvi, 1996, *Seismic Design and Retrofit of Bridges*, John Wiley and Sons, ISBN 0-57998-X.
- Polyakov, S.V., 1960, "On the Interaction Between Masonry Filler Walls and Enclosing Frame When Loaded in the Plane of the Wall," *Translations in Earthquake Engineering Research Institute*.
- Restrepo, J. and B. DeVino, 1996, "Enhancement of the Axial Load Carrying Capacity of Reinforced Concrete Columns by Means of Fiber-glass Epoxy Jackets," *Proceedings of the Advanced Composite Materials in Bridges and Structures II*, Montreal, Quebec, pp 547-553.
- Stafford-Smith, B. and C. Carter, 1969, "A Method of Analysis for Infilled Frames," *Proceedings of the Institution of Civil Engineers*, Vol. 44.
- Stafford-Smith, B., 1966, "Behavior of Square Infilled Frames," *Journal of the Structural Division*, ASCE, Vol. 92, February 1966.
- Stafford-Smith, B., 1962, "Lateral Stiffness of Infilled Frames," *Journal of the Structural Division*, ASCE, Vol. 88, December 1962.
- Triantafillou, T.C., 1998a, "Shear Strengthening of Reinforced Concrete Beams Using Epoxy-Bonded FRP Composites," *ACI Structural Journal*, V. 95, No. 2, pp. 107-115.
- Triantafillou, T.C., 1998b, "Strengthening of Structures with Advanced FRPs," *Progress in Structural Engineering and Materials*, V. 1, pp 126-134.
- Triantafillou, T.C., 1998c, "Strengthening of Masonry Structures Using Epoxy-Bonded FRP Laminates," *Journal of Composites for Construction*, 2: 96-104.

Uncited

- Al-Chaar, G., D. Abrams, G. Lamb, and J. Trovillion, 2002, "Rehabilitation of Infilled Nonductile Concrete Frames using Fiber Reinforced Polymer," *Proceedings of the Third International Conference on Composites in Infrastructure*, University of Arizona, Tucson, AZ, June 2002.
- Al-Chaar, G. and D. Abrams, 2001, "Parametric Studies on Seismic Behavior of Frame-Infill Systems," *Proceedings of the Ninth Canadian Masonry Symposium*, New Brunswick, Canada, June 2001.

Al-Chaar, G., G. Lamb, and D. Abrams, 2001, "Seismic Behavior of a Multistory and Multibay Frame-Infill System," *Proceedings of the Ninth Canadian Masonry Symposium*, New Brunswick, Canada, June 2001.

Applied Technology Council (ATC), "Seismic Evaluation and Retrofit of Concrete Buildings," Volume 1, ATC-40 Report, ATC, Redwood City, CA, 1996.

FEMA 274, *NEHRP Commentary on the Guidelines for the Seismic Rehabilitation of Buildings*, FEMA, October 1997.

SAP 2000 v7.0, "Integrated Finite Elements Analysis and Design of Structures," Computers and Structures, Inc., Berkeley, CA, 1998.

Appendix A: 3x3 Full-Scale Example

This illustrative example details the procedure for estimating the ultimate base shear capacity, deflection at ultimate capacity, and initial stiffness for an infilled R/C frame rehabilitated with FRP using a pushover analysis.

This example structure is a full-scale, 3-story 3-bay R/C frame rehabilitated with FRP. The frame is partially infilled with door and window openings in the lower left panel, with the remainder of the panels fully infilled. The infill has been rehabilitated with FRP using X frame strip orientation on every fully infilled panel, while the perforated panel used picture frame orientation. The columns have been fully wrapped with FRP and the T-beams have been U-wrapped. The structure is assumed to be new, with no existing infill damage. Figure A.1 shows an elevation view of the frame, while Table A.1 lists the dimensional and physical properties of the frame, FRP, infill panel, and openings.

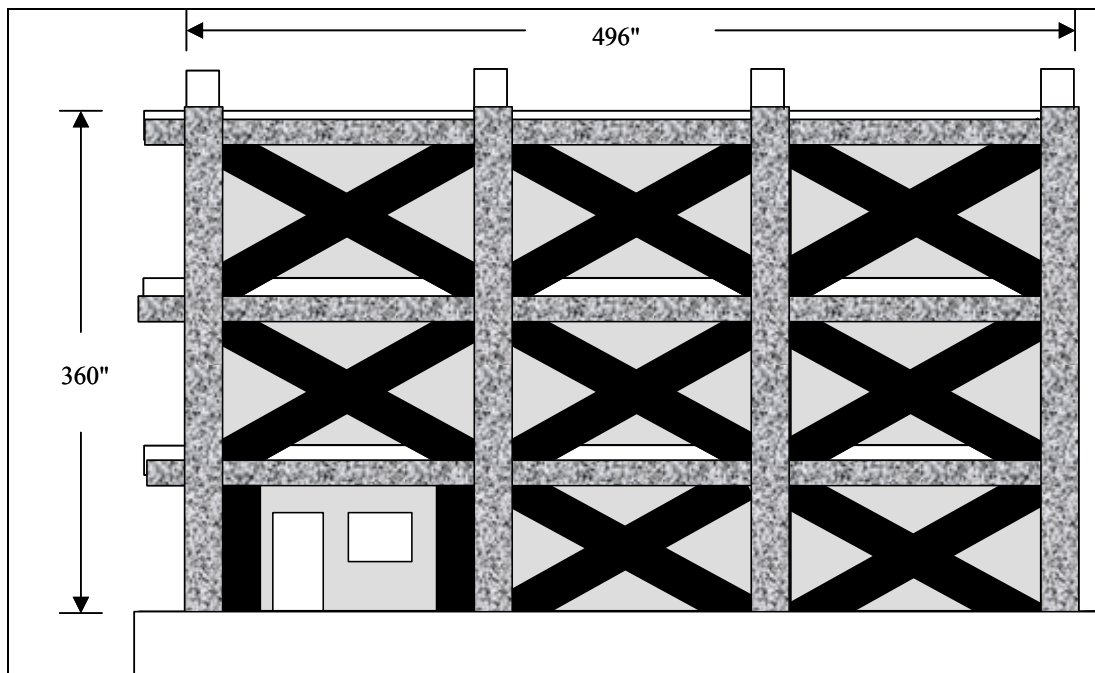


Figure A.1. Elevation view of building.

Table A.1. Properties of the frame, FRP, infill, and openings.

Frame			FRP			Infill		
f'_c	5.575	ksi	t_f	0.0026	in	E_m	5.575	ksi
ϵ_{cu}	0.003	in/in	n	1	plies	f'_m	0.003	ksi
h	17	in	C_E	0.95	-	f'_v	0.265	ksi
b (col)	10	in	ϵ'_{bi}	0	in/in	A_n	270.7	in ²
b (beam)	72	in	ϵ_{bi}	0	in/in	H	120	in
f_y	60	ksi	Openings			h_m	104.5	in
E_s	29000	ksi	h_{door}	78 ^{7/16}	in	l	144	in
$A_{s'}$	1.6	in ²	b_{door}	32	in	t	8	in
A_s	0.93	in ²	h_{window}	43.5	in	t_{eff}	1.88	in
A_{st}	1.76	in ²	b_{window}	48	in	D	177.92	in
d'	1.5	in	A_{panel}	15,048	in ²	θ	0.943	rad
d	15.5	in	A_{open}	4,598	in ²	-	-	-

Step 1. Determine the FRP Design Strength Curve

Figure A.1 shows the average FRP stress-strain curve, which was determined from testing FRP coupons.

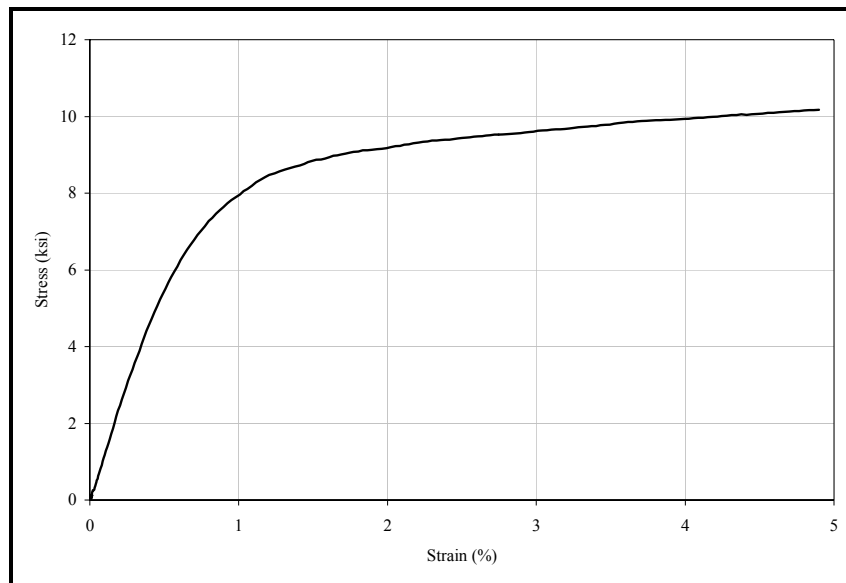


Figure A.1. Average FRP stress-strain curve.

Once determining the average FRP stress-strain characteristics, a bilinear representation of the curve should be constructed. Figure A.2 shows the yield and ultimate rupture strain of the FRP as well as the initial and secondary moduli.

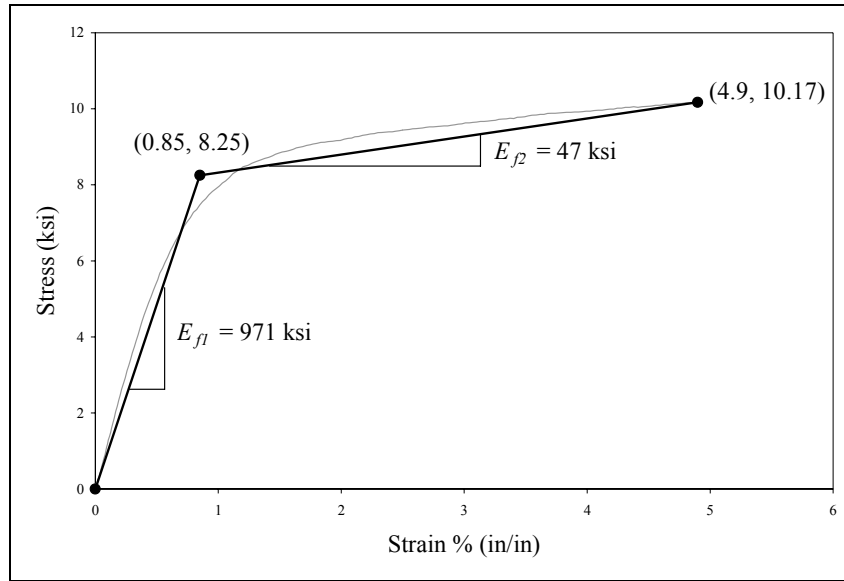


Figure A.2. Bilinear FRP stress-strain curve.

The FRP system being used in this example is carbon/epoxy used in the interior of the building. Therefore, the value of C_E is 0.95 from Table 2. Using this value, the FRP properties to be used in the structural evaluation can be determined (Eq A.1). The resulting FRP design strength curve is shown in Figure A.3.

$$\begin{aligned}
 f_{fy} &= 0.95 * 8.25 = 6.19 & \epsilon_{fy} &= 0.95 * 0.0085 = 0.0064 \\
 f_{fu} &= 0.95 * 10.17 = 9.66 & \epsilon_{fu} &= 0.95 * 0.0490 = 0.0465
 \end{aligned}$$

Eq A.1

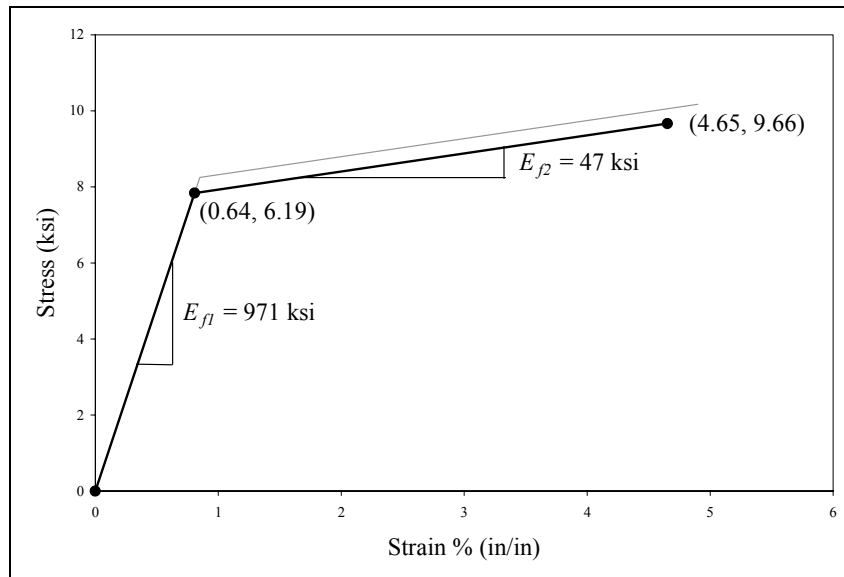


Figure A.3. FRP design strength curve.

Step 2. Determine the Moment-Curvature Behavior

Once the FRP design strength curve has been generated, the nominal moment capacity can be determined. Equations 4 – 12 must be solved simultaneously to maintain equilibrium and strain compatibility. Then Equation 3 can be used to calculate M_n . For the example problem, Equation A.2 yields the nominal moment capacity.

$$\begin{aligned} M_n &= 0.93 * 60 * (15.5 - 0.31) + 1.6 * (-15.8) * (0.31 - 1.5) \\ &+ 0.95 * 0.187 * 7.4 * (17 - 0.31) + 0.85 * 5.575 * 0.77 * 0.31 * 72 * \left(1 - \frac{0.77}{2}\right) \\ &= 950 \text{ k-in.} \end{aligned} \quad \text{Eq A.2}$$

Next, the flexural yield point of the member can be determined using Equation 14 and the stress-strain distribution in Figure 9. Therefore, M_y , for this example, is calculated from Equation A.3.

$$\begin{aligned} M_y &= \frac{72 * 1.56^2}{3} * 0.994 + 1.6 * 0.25 * (1.56 - 1.5) + 0.93 * 60 * (15.5 - 1.56) \\ &+ 0.95 * 0.187 * 2.23 * (17 - 1.56) = 843 \text{ k-in.} \end{aligned} \quad \text{Eq A.3}$$

The curvature at yield and nominal moment are given by Equations 15 and 16. Equations A.4 and A.5 show these calculations for the example problem.

$$\phi_y = \frac{0.0021}{15.5 - 1.56} = 1.51 * 10^{-4} \text{ rad/in.} \quad \text{Eq A.4}$$

$$\phi_n = \frac{0.007}{15.5 - 1.56} = 5.02 * 10^{-4} \text{ rad/in.} \quad \text{Eq A.5}$$

Using these values, a simplified moment-curvature graph can be constructed as shown in Figure A.4.

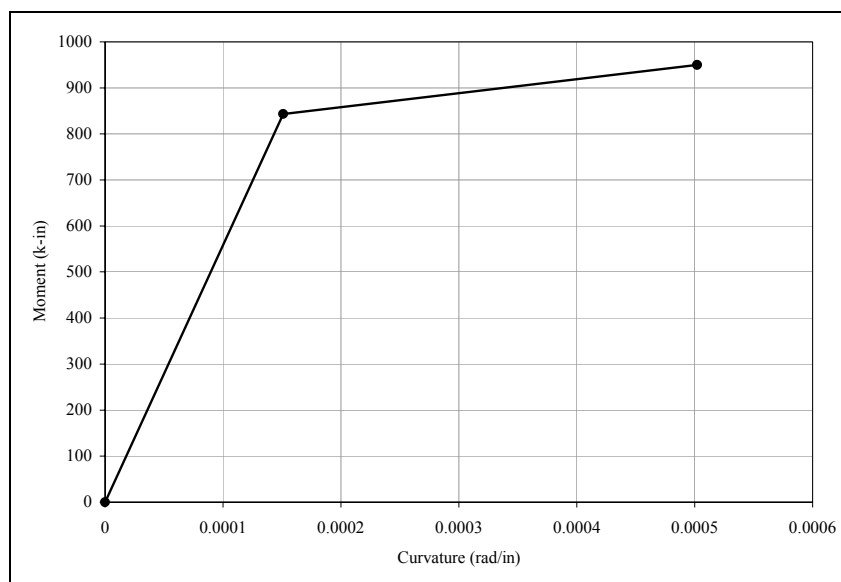


Figure A.4. Moment-curvature behavior.

Step 3. Determine Shear Capacity

The first step in determining shear capacity of the rehabilitated frame members is to determine the concrete and steel contributions as shown in Equations A.6 and A.7. The steel shear reinforcement consists of #3 bars at 10-in. spacing.

$$V_c = 2b_w d \sqrt{f'_c} = 2 * 10 * 15.5 * \frac{\sqrt{5575}}{1000} = 23.15 \text{ kips} \quad \text{Eq A.6}$$

$$V_s = \frac{A_v f_y d}{s} = \frac{2 * 0.11 * 60 * 15.5}{10} = 20.46 \text{ kips} \quad \text{Eq A.7}$$

The following steps illustrate how to determine the FRP contribution to shear resistance. Equation A.8 determines the area of FRP shear reinforcement, while Equation A.9 computes the effective stress in the FRP. The effective strain in the FRP is taken as the recommended value of 0.004.

$$A_{fv} = 2nt_f w_f = 2 * 1 * 0.026 * 12 = 0.624 \text{ sq in} \quad \text{Eq A.8}$$

$$f_{fe} = E_{f1} \epsilon_{fu} = 971 * 0.004 = 3.884 \text{ ksi} \quad \text{Eq A.9}$$

The FRP contribution to shear strength can now be found using Equation A.10. Since the FRP was bonded to the members as one continuous strip, the width and spacing of the FRP were set to the same arbitrary value, in this case 12 inches. In

addition the slab thickness was 6 in., so the depth of the FRP was 9.5 in. (15.5 in. - 6 in.).

$$\psi_f V_f = \frac{0.85 A_{fv} f_{fe} (\sin \alpha + \cos \alpha) d_f}{s_f} = \frac{0.85 * 0.624 * 3.884 * 1 * 9.5}{12} = 1.63 \text{ kips} \quad \text{Eq A.10}$$

The nominal shear capacity can now be computed using Equation A.11.

$$V_n = V_c + V_s + \psi_f V_f = 23.15 + 20.46 + 1.63 = 45.24 \text{ kips} \quad \text{Eq A.11}$$

Step 4. Determine Moment-Thrust Interaction

To determine the moment-thrust interaction, the nominal axial capacity must be computed. The first step is to calculate the radius of the edges of the section as shown in Equation A.12.

$$r = \sqrt{\left(\frac{b}{2}\right)^2 + \left(\frac{h}{2}\right)^2} = \sqrt{\left(\frac{10}{2}\right)^2 + \left(\frac{17}{2}\right)^2} = 9.86 \text{ in} \quad \text{Eq A.12}$$

The longitudinal steel reinforcement ratio must also be found using Equation A.13.

$$\rho_g = \frac{A_{st}}{A_g} = \frac{1.76}{170} = 0.01035 \quad \text{Eq A.13}$$

Using these two parameters, the efficiency factor for confinement can be calculated following Equation A.14.

$$\kappa_a = 1 - \frac{(b-2r)^2 + (h-2r)^2}{3bh(1-\rho_g)} = 1 - \frac{(10-2*9.86)^2 + (17-2*9.86)^2}{3*10*17(1-0.01035)} = 0.798 \quad \text{Eq A.14}$$

Since the columns in this example are rectangular, the reinforcement ratio for non-circular sections must be used (Eq A.15).

$$\rho_f = \frac{2nt_f(b+h)}{bh} = \frac{2*1*0.0026(10+17)}{10*17} = 0.000826 \quad \text{Eq A.15}$$

Now, the confining pressure due to the FRP jacket can be determined from Equation A.16. Note that the effective strain used was 0.004 as recommended by ACI 440.

$$f_l = \frac{\kappa_a \rho_f \varepsilon_{fe} E_{f1}}{2} = \frac{0.798 * 0.000826 * 0.004 * 971}{2} = 0.00128 \quad \text{Eq A.16}$$

Next, the confined concrete compressive strength can be calculated following Equation A.17.

$$\begin{aligned} f'_{cc} &= f'_c \left[2.25 \sqrt{1 + 7.9 \frac{f_l}{f'_c}} - 2 \frac{f_l}{f'_c} - 1.25 \right] \\ &= 5.575 \left[2.25 \sqrt{1 + 7.9 \frac{0.00128}{5.575}} - 2 \frac{0.00128}{5.575} - 1.25 \right] = 5.583 \text{ ksi} \end{aligned} \quad \text{Eq A.17}$$

Finally, the nominal axial compression capacity can be calculated using Equation A.18.

$$\begin{aligned} P_n &= 0.85 \psi_f f'_{cc} (A_g - A_{st}) + f_y A_{st} \\ &= 0.85 * 0.95 * 5.583 (170 - 1.76) + 60 * 1.76 = 864 \text{ kips} \end{aligned} \quad \text{Eq A.18}$$

Now that the compressive strength has been determined, the nominal axial tension capacity should be found using Equation A.19. Again, note that the effective strain used was the recommended value of 0.004 from ACI 440.

$$T_n = A_{st} f_y + \psi_f A_f E_{f1} \varepsilon_{fe} = 1.76 * 60 + 0.95 * 0.1404 * 971 * 0.004 = 106 \text{ kips} \quad \text{Eq A.19}$$

Once the nominal compressive, tensile, and flexural capacities have been determined, the remaining points on the interaction diagram can be found. Figure A.5 shows the interaction diagram for the example problem.

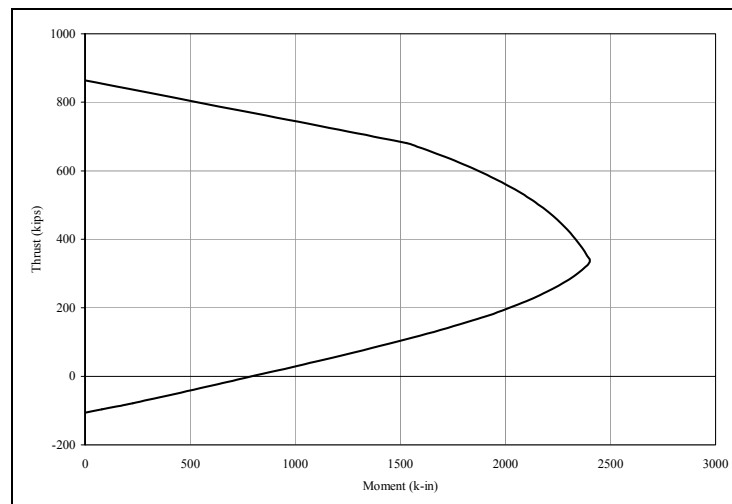


Figure A.5. Thrust-moment interaction diagram.

Step 5. Determine Properties of Equivalent Strut

After modeling the frame, the equivalent eccentric diagonal struts are added to represent the masonry infill. Since most of the panels are fully infilled, the struts should, at first, be designed to represent full infill panels, then multiplied by a proper reduction factor to account for any openings in the infill panel.

The equivalent strut width is evaluated by first using Equation 39 to calculate the parameter $\lambda_1 H$, as shown in Equation A.20. $\lambda_1 H$ is then inserted into Equation 40 to determine the equivalent strut width, a , as illustrated in Equation A.21. Since the infill panels are assumed to be undamaged, R_2 is taken to be 1.0.

$$\lambda_1 H = 120 \left[\frac{2200 * 8 * \sin(2 * 0.943)}{4 * 4300 * 3413 * 104.5} \right]^{1/4} \quad \text{Eq A.20}$$

$$\Rightarrow \lambda_1 H = 4.877$$

$$a = 0.175 * 177.92 (4.877)^{-0.4} \quad \text{Eq A.21}$$

$$\Rightarrow a = 16.52 \text{ in.}$$

Next, the eccentric placement for the strut must be determined by calculating the distance (l_{column}). The distance (l_{column}) is found by simultaneously solving Equations 42 and 43 for l_{column} and θ_{column} , as shown in Equation A22.

$$l_{column} = \frac{16.52}{\cos(\theta_{column})}$$

$$\tan(\theta_{column}) = \frac{104.5 - \frac{16.52}{\cos(\theta_{column})}}{144} \quad \text{Eq A.22}$$

$$\Rightarrow l_{column} = 19.20 \text{ in.}$$

$$\Rightarrow \theta_{column} = 0.535 \text{ rad}$$

The equivalent diagonal struts should therefore be placed at a distance of 19.20 in. along the column from the beam-column joints with moment releases at each end. The strut should be defined as a concrete material with the same material properties as the masonry panel.

Next, a strut reduction factor, $(R_1)_i$, is applied to represent the bottom-left panel with door and window openings. This factor is computed using Equation 44, as shown in Equation A.23.

$$\begin{aligned} (R_1)_i &= 0.6 \left(\frac{4598}{15048} \right)^2 - 1.6 \left(\frac{4598}{15048} \right) + 1.0 \\ \Rightarrow (R_1)_i &= 0.567 \end{aligned} \quad \text{Eq A.23}$$

Then the modified strut width is calculated from Equation 41, as shown in Equation A.24. Note that the value for the FRP strength increase factor, ξ_I , was 1.48 (taken from Table 5).

$$\begin{aligned} a_{\text{mod}} &= 16.52 * (0.567) * (1.0) * (1.48) \\ \Rightarrow a_{\text{mod}} &= 13.86 \text{ in.} \end{aligned} \quad \text{Eq A.24}$$

Next, plastic hinges are defined to represent possible failure points for the frame. Hinges controlled by the combination of axial, moment, and shear forces are placed at a distance (l_{column}) from the joints along the columns. Conversely, hinges along the beam account for only moment and shear forces, and are placed at a distance (l_{beam}) from the joints. This distance (l_{beam}) is calculated by simultaneously solving Equations 49 and 50, as shown in Equation A.25.

$$\begin{aligned} l_{\text{beam}} &= \frac{16.52}{\sin(\theta_{\text{beam}})} \\ \tan(\theta_{\text{beam}}) &= \frac{104.5}{144 - \frac{16.52}{\sin(\theta_{\text{beam}})}} \\ \Rightarrow l_{\text{beam}} &= 25.03 \text{ in.} \\ \Rightarrow \theta_{\text{beam}} &= 0.721 \text{ rad} \end{aligned} \quad \text{Eq A.25}$$

Axial hinges are placed at the midpoints of the struts. Figure A.6 shows the hinge types and placement around a generic panel.

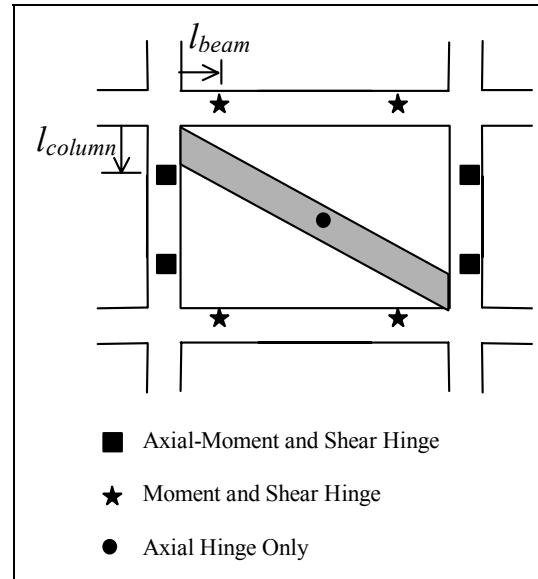


Figure A.6. Plastic hinge placement.

Upon placement of the hinges, the capacity of the strut hinges (R_{strut}) should be computed. The compressive strength (R_{strut}) should be calculated using Equations 45 – 48, as illustrated in Equations A.26 – A.29.

$$R_{cr} = 13.86 * 1.88 * 2.505$$

$$\Rightarrow R_{cr} = 65.3 \text{ kips}$$
Eq A.26

$$R_{shear} = 270.7 * 0.265 * 1 * 1$$

$$\Rightarrow R_{shear} = 71.7 \text{ kips}$$
Eq A.27

$$\tan(\theta_{strut}) = \frac{104.5 - 2 * 19.20}{144}$$

$$\Rightarrow \theta_{strut} = 24.66^\circ$$
Eq A.28

$$R_{strut} = \min \left\{ \begin{array}{l} 77.8 \text{ kips} \\ 71.7 / \cos(24.66^\circ) = 78.9 \text{ kips} \end{array} \right\}$$

$$\Rightarrow R_{strut} = 77.8 \text{ kips}$$
Eq A.29

Next, rigid end offsets (REOs) are placed to increase the rigidity of the joints, as well as ensure that the maximum stresses computed are located at the defined plastic hinges. The REOs should have a rigid zone factor of one and span from the beam column joints outward to a distance (l_{beam}) along the beams and a distance (l_{column}) along the column.

Finally, the load and pushover cases are defined. The pushover is defined using the local redistribution member unloading method, with gravity loads as an initial condition. The inertia force distribution used for this example is an inverted triangle. Although more than one inertia force distribution is recommended, for simplicity only one is used in this example.

Step 6: Analyze Results

After running the static pushover analyses, the lateral load capacity is determined to be 269 kips. The pushover curve is illustrated in Figure A.7.

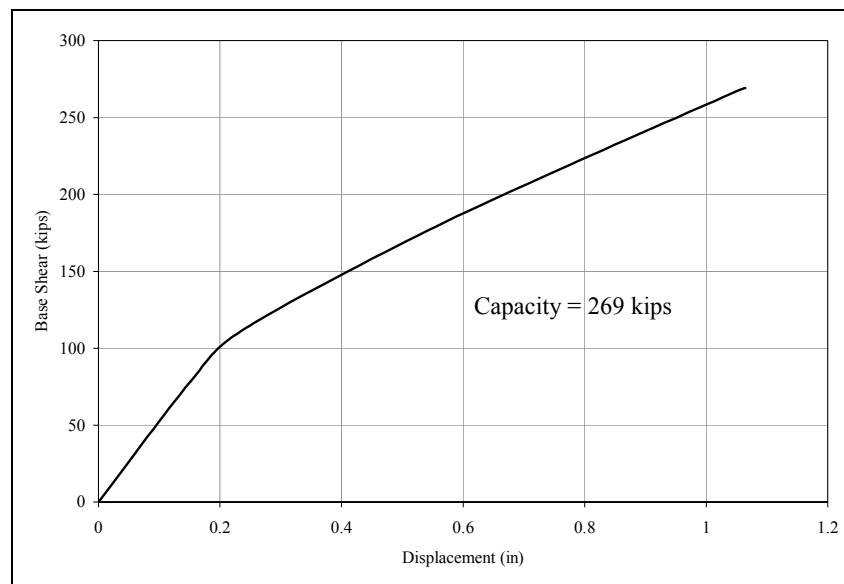


Figure A.7. Case I pushover curve.

The next step is to simplify the pushover curve as a bilinear curve with initial and post-yield stiffness values, as well as well-defined yield and ultimate values. Figure A.8 shows a plot of the original pushover curve and its corresponding bilinear estimation.

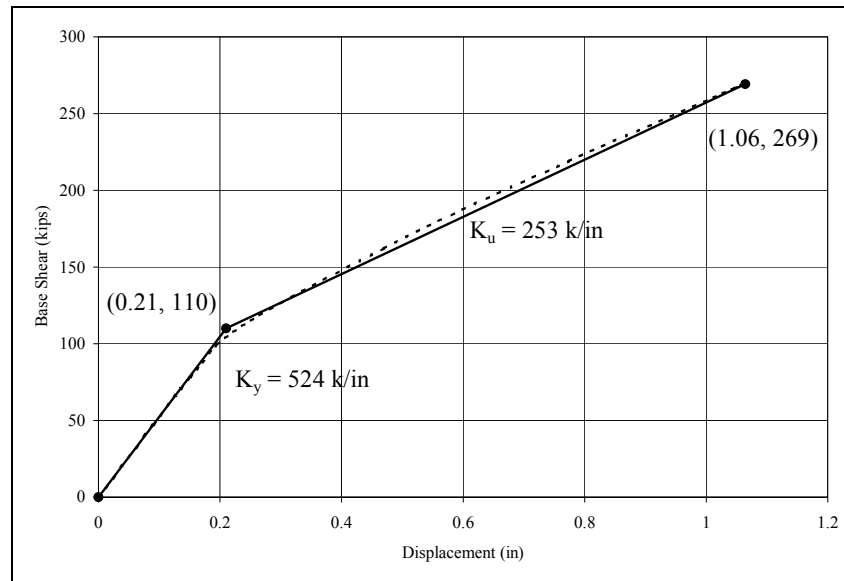


Figure A.8. Bilinear estimation.

Also shown in Figure A.8 are the initial and post-yield bilinear stiffness values for the estimated curve. For this example, it is satisfactory to use the initial stiffness value predicted using the Mainstone (1971) equations since the aspect ratio (I/h) of the panels in this frame is 1.38 (between 0.67 and 1.5).

The modified initial and post-yield stiffness are found from Equations 54 and 55. The values of K_i and K_f for the example problem are computed from Equations A.30 and A.31. Note that the Stafford-Smith and Carter (1969) equivalent strut width in Equation 54 could also be used as an alternate value for K_i .

$$K_i = 3 * 524 = 1572 \text{ k / in.} \quad \text{Eq A.30}$$

$$K_f = 2 * 253 = 506 \text{ k / in.} \quad \text{Eq A.31}$$

Assuming the value for K_i to be 1,572 k/in., the new stiffness values are then applied, along with the estimated yield and ultimate base shear values from Figure A.8, to generate the modified bilinear plot depicted in Figure A.9. This plot should predict the in-plane ultimate capacity and displacement at ultimate capacity with reasonable accuracy.

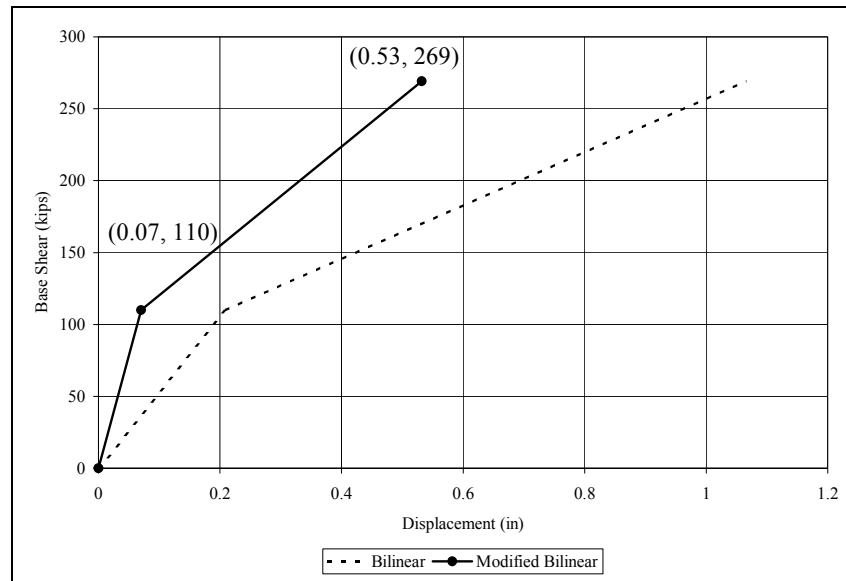


Figure A.9. Modified bilinear curve.

Figure A.10 illustrates the effectiveness of the rehabilitation scheme by comparing the structure with FRP overlay to the original structure.

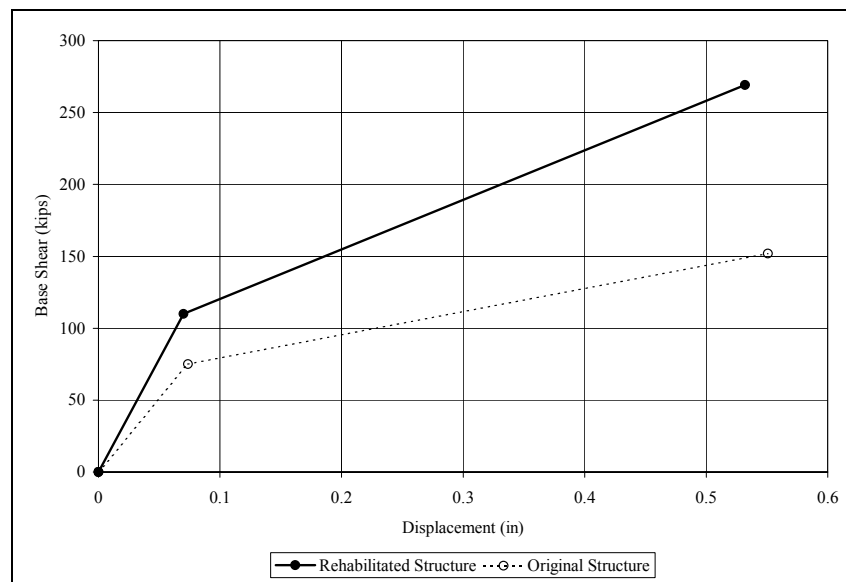


Figure A.10. Pushover curve comparison between rehabilitated and original structure.

Appendix B: Commentary on Selected Sections

Flexural Capacity of R/C Frame Members Rehabilitated With FRP

Four beams were fabricated and tested in flexure with the properties listed in Table B.1. Two of these beams had no FRP while the other two were fully wrapped. The FRP was composed of carbon fibers oriented at 0°/90°. The FRP strength reduction factors ψ , C_E , ϕ were set to unity to reflect the controlled laboratory conditions. The initial strains in the reinforcing steel, ε'_{bi} and ε_{bi} , were set to zero since there was not any significant load on the members prior to testing.

Table B.1. Properties of the experimental beams fully wrapped with FRP tested in flexure.

f'_c	6.5	ksi	f_y	56	ksi
ε_{cu}	0.003	in/in	E_s	29000	ksi
h	7.75	in	A_s'	0.22	in ²
b	5	in	A_s	0.22	in ²
t_f	0.0026	in	d'	1.125	in
ε_{fu}	0.0158	in/in	d	6.625	in
E_f	33500	ksi	ε'_{bi}	0	in/in
n	1	plies	ε_{bi}	0	in/in
κ_m	0.9	-	ψ	1	-
C_E	1	-	ϕ	1	-

Table B.2 summarizes the experimental and theoretical results of the flexural testing. Tests 1 and 2 refer to the individual test results for each of the two specimens: fully wrapped and no FRP. The average experimental moment capacity is the average of tests 1 and 2. The first column indicates the FRP location on the beam. Figure B.1 illustrates the nomenclature used to describe the FRP location. There are no experimental results for FRP bonded to the bottom face, below the neutral axis, or below the top face. However, theoretical values for moment capacity were calculated to compare to experimental results. The last column indicates the ratio of the theoretical to experimental moment capacity.

The ratio of theoretical to experimental moment capacity for the control beams without FRP was 81.3 percent. To keep the same amount of reliability when FRP is fully wrapped around the beams, the theoretical moment capacity for this case should also yield a ratio of 81.3 percent. However, when considering all of the FRP for the fully wrapped case effective in flexure, the ratio was 1.074. This indicates that the theoretical moment capacity was greater than the experimental.

A theoretical exercise was performed to calculate the moment capacities of beams with FRP bonded to the bottom face, below the neutral axis, and below the top face in order to compare to the experimental value for the fully wrapped case. For the FRP locations below neutral axis and below top face, the theoretical moment capacities were within 1 percent of the fully wrapped case. This means that the theoretical values for these two cases were still overstating the actual moment capacity. However, the theoretical moment capacity considering only the FRP bonded to the bottom face effective in resisting flexural loads was 124.2 kip-in. This yielded a ratio of 0.818, which was within 0.6 percent of the ratio calculated for the control beam without FRP. Therefore, when considering only the FRP bonded to the bottom face of the member effective in flexure, the reliability between the theoretical moment capacity of the control beam without FRP compared to the beam fully wrapped with FRP remained constant. Using this research as a basis, this report recommends considering only the FRP bonded to the bottom face of the member effective in resisting flexure.

Table B.2. Experimental and theoretical moment capacities.

FRP Location on Beam	Test 1 Moment Capacity (k-in)	Test 2 Moment Capacity (k-in)	Average Experimental Moment Capacity (k-in)	Theoretical* M_n (k-in)	Ratio**
None	94.9	106.8	100.8	82.0	0.813
Bottom Face Only	-	-	-	124.2	0.818
Below Neutral Axis	-	-	-	161.6	1.065
Below Top Face	-	-	-	161.8	1.066
Fully-Wrapped	158.6	144.9	151.7	163.0	1.074

* The theoretical moment strength was calculated with the FRP reduction variables Ψ and C_E set to unity.

** For cases without experimental results, the average experimental moment strength was based on the fully-wrapped case.

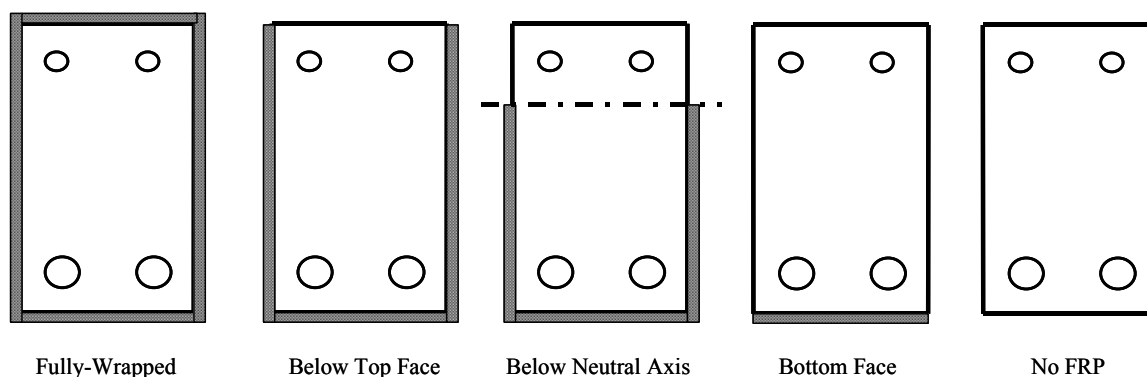


Figure B.1. Nomenclature used to describe location of FRP bondage.

The above research indicates that, for an R/C beam fully wrapped with FRP and the additional strength reduction factor, ψ , set to unity, considering only the FRP bonded to the bottom face of the member effective in resisting flexural loads will yield accurate strength predictions with the same reliability as “bare” R/C members. ACI 440 recommends using $\psi = 0.85$ for R/C members with FRP bonded to the bottom (tension) face only. Therefore, the additional strength reduction factor must be a function of the FRP wrapping scheme. This document recommends using the values in Table B.3 for ψ_f .

Table B.3. Values of ψ_f for different FRP wrapping schemes.

Wrapping Scheme	ψ_f
Fully-Wrapped	1.00
U-Wrap	0.95
Tension Face Only	0.85

Furthermore, this document discourages the use of FRP bonded only to the tension face of the member. With the increase in flexural capacity from the addition of FRP, shear failure becomes the predominant mode of failure. In addition, the probability of FRP debonding, FRP rupture, or cover delamination is much higher when the FRP is bonded only to the tension face of the member. The recommended wrapping scheme should be to fully wrap the member when possible. In most situations, however, a U-wrap is the only economical and practical wrapping scheme.

Axial Capacity of R/C Frame Members Rehabilitated with FRP

Two rectangular columns fully wrapped with FRP were tested in compression to verify the equations contained in this document. These columns possessed the same dimensions and material properties as those listed in Table B.1 except that the total

area of steel, A_{st} , was equal to 0.44 sq in. Table B.4 summarizes the experimental and theoretical compressive capacities.

Table B.4. Experimental and theoretical axial capacities.

Specimen	Experimental Axial Capacity (kips)	Theoretical Axial Capacity (kips)	Ratio
Bare	265.0	236.3	0.892
Fully-Wrapped	300.5	256.8	0.854

In both cases, the theoretical strength was between 85 and 90 percent of the experimental capacities. The ratio of theoretical to experimental axial capacity for both cases was within 5 percent. Therefore, the equations contained in this document for determining the axial strength of R/C members confined with FRP not only accurately predict the strength, but also maintain the same amount of reliability as the traditional equations give for plain R/C members.

Moment-Thrust Interaction of R/C Frame Members Rehabilitated With FRP

Figure B.2 shows the interaction curves for a bare column, a column fully wrapped with FRP assuming only the FRP bonded to the tension face of the member is effective in resisting flexural loads, and a column fully wrapped assuming 100 percent of the FRP is effective in resisting flexural loads. The column was analyzed with the same dimensions and material properties as listed in Table B.1, except the total area of steel was equal to 0.44 sq in.

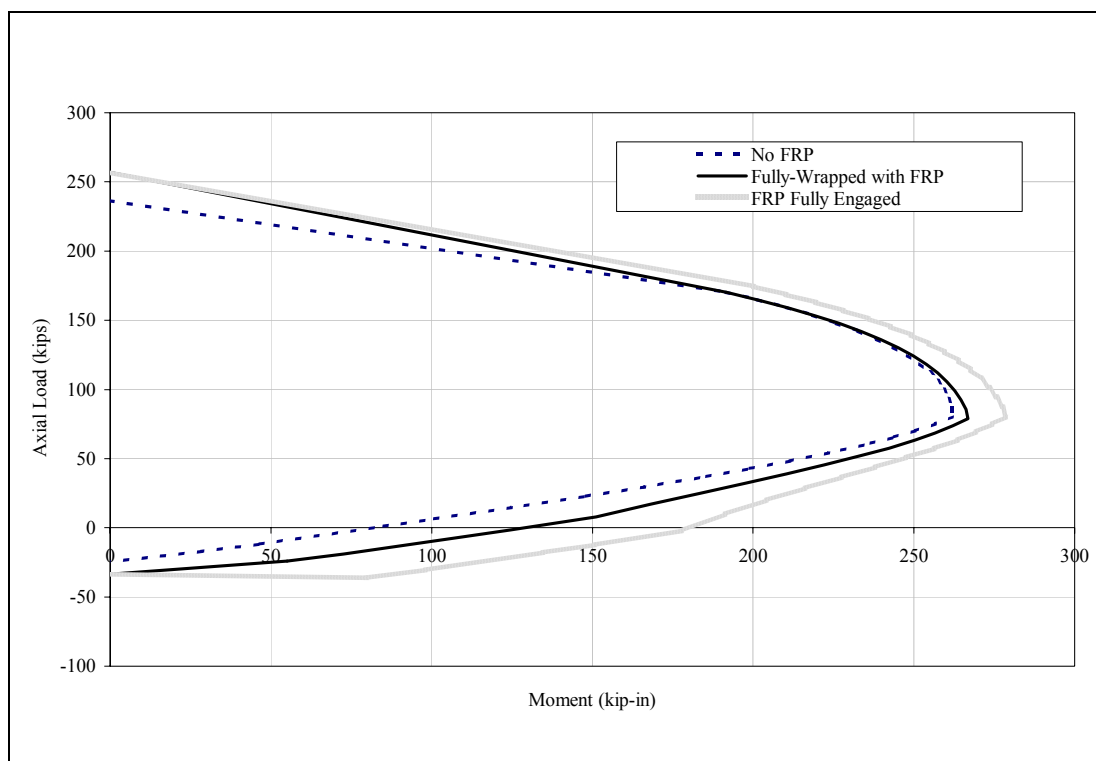


Figure B.2. Thrust-moment interaction curve.

The curve labeled “FRP Fully Engaged” clearly shows that the nominal moment capacity is too large using this assumption (180 k-in. >> 125 k-in.). This point was proven in the section regarding flexural capacity of members strengthened with FRP. However, the “FRP Fully Engaged” curve does illustrate a smoother transition between pure axial compression and pure flexure (i.e., does not merge with the “No FRP” curve). Once equations are developed to account for the *combination* of confinement and stress-strain resistance when members are under combined axial and flexural loads, the curve labeled “Fully-Wrapped with FRP” will also show greater capacity than the bare member under all load combinations. Also, note that the fully engaged curve does not show a smooth transition to the pure tension condition. This is due to the limitation of ϵ_{te} prescribed by ACI 440 for tensile capacity.

Strength and Stiffness of URM Infill Rehabilitated With FRP

Fourteen infill walls constructed of full-scale CMU were rehabilitated with FRP. Table B.5 lists the FRP system, FRP pattern, fiber bias, number of plies, ultimate tensile strength of FRP, initial modulus of FRP elasticity, and mortar cube strength for each of the walls tested. Note that walls #7 and #11 are the control specimens. Figure B.3 shows the FRP strip and URM panel dimensions of the test specimens.

Table B.5. Material properties for the CMU walls rehabilitated with FRP.

Wall Number	FRP System	FRP Pattern	Fiber Bias	Number of Plies	f_{fu}^* (ksi)	E_{f1} (ksi)	Mortar Cube Strength (psi)
1	9.5 oz. Bi-directional	Full	0-90	3	17.8	603	1878
							1927
2	27 oz. Uni-directional	Full	0	1	62.06	1773	1900
							1749
3	27 oz. Uni-directional Glass	Reinforced Picture Frame	0	1	62.06	1773	1749
			0	2	69.83	1365	1495
			0	3	-----	-----	1204
4	27 oz. Uni-directional Glass	Reinforced X-Frame	0	1	62.06	1773	1670
			+/-45	1	-----	-----	1706
			+/-45	2	-----	-----	-----
5	9.5 oz. Bi-directional	X frame	+/-45	3	9.7	357	1706
			+/-45	6	-----	-----	1714
6	9.5 oz. Bi-directional	Picture Frame	0-90	3	17.8	603	1814
							1807
7	N/A	Control	N/A	N/A	N/A	N/A	1807
							1447
8	27 oz. Uni-directional	Full	0	2	69.83	1365	1748
							2142
9	27 oz. Uni-directional	H-frame	0	1	62.06	1773	2142
			90	1	3.41	1001	1973
10	27 oz. Uni-directional	Picture Frame	0	1	62.06	1773	2152
							2310
11	N/A	Control	N/A	N/A	N/A	N/A	2310
							2034
12	27 oz. Uni-directional	X-frame	+/-45	2	-----	-----	1837
			+/-45	4	-----	-----	2341
13	27 oz. Uni-directional	X-frame	+/-45	1	-----	-----	2341
			+/-45	2	-----	-----	1663
14	27 oz. Uni-directional	Picture Frame	0	2	69.83	1365	2097
							1973

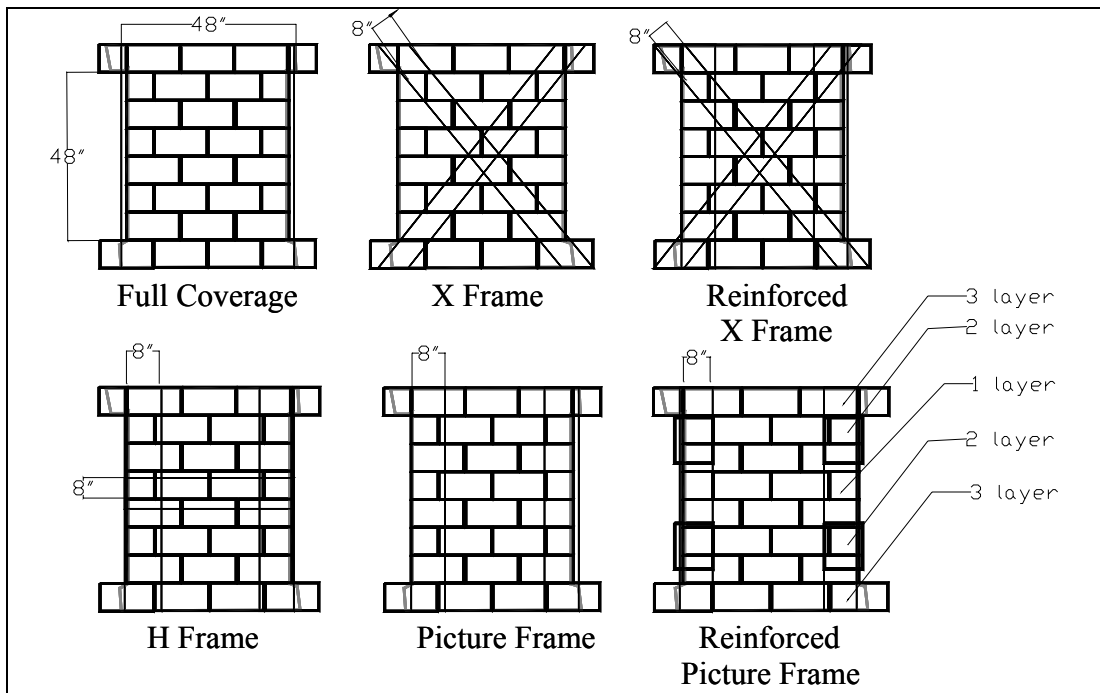


Figure B.3. Dimensions of URM panel and FRP strips.

These masonry walls were cyclically tested to determine the effectiveness of the FRP wrapping schemes with respect to strength and stiffness. Figure B.4 illustrates the peak load and corresponding displacement for each of the masonry walls tested. The FRP strength and stiffness increase factors (ξ_1 and ξ_2 , respectively) were derived from these data.

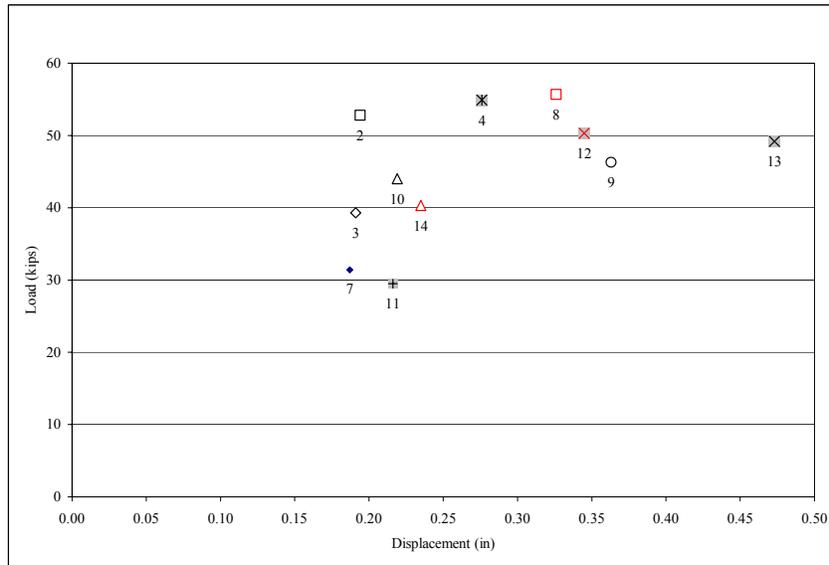


Figure B.4. Peak load and corresponding displacement for CMU walls.

Glossary

Definitions

AFRP: Aramid fiber-reinforced polymer.

Aramid Fiber: Aromatic polyamide fiber with high strength and stiffness.

Axial Hinge: A plastic hinge defined to model the inelastic action of a structural member when its yield strength is surpassed due to axial forces.

Axial-Moment Hinge: A plastic hinge defined to model the inelastic action of a structural member when its yield strength is surpassed due to the combination of axial loads and bending moments.

Building Type: A building classification defined by FEMA 310 that groups together building types with common lateral force resisting systems.

Carbon Fiber: Highly anisotropic fiber formed from long bundles of linked graphite plate.

CFRP: Carbon fiber-reinforced polymer.

Composite: A combination of two or more materials.

Concrete Substrate: The concrete surface underlying the FRP system.

Coupon: FRP tensile test specimen used to determine f_{tu}^* and ϵ_{tu}^* .

Debonding: Separation between the concrete substrate and the FRP.

Delamination: Separation between the individual layers of FRP.

Design Flexural Capacity: The nominal moment capacity, ϕ , multiplied by the strength reduction factor, M_n .

E-Glass: A general purpose fiber with electrical properties, strength, and durability appropriate for many applications.

Epoxy: Any of various, usually thermosetting, resins used in surface coatings, as matrix resins for composites, and as structural adhesives.

Existing Infill Damage: Damage experienced by the infill during its service life.

Fiber: A filamentary material.

Fiber Content: The amount of fiber present in a composite usually expressed as a percentage volume fraction.

Flexural Design Rupture Strain: The design rupture strain, ϵ_{fu} , multiplied by the bond-dependent coefficient for flexure, κ_m .

Fiber-Reinforced Polymer (FRP): Composite material made up of a polymer matrix reinforced with fibers.

Frame: A structural system of beams and columns that resists vertical/lateral loads.

FRP System: The composite FRP material composed of fibers and resin.

GFRP: Glass fiber-reinforced polymer.

Glass Fiber: Fiber formed from molten glass.

Gross Laminate Area: The total cross-sectional area of the cured FRP system including all fibers and resin.

Infill Aspect Ratio: Ratio of full length to height dimensions for masonry infill panels (l/h_m).

Infill Slenderness Ratio: Ratio of full height to thickness dimensions for masonry infill panels (h_m/t).

Infill Strength: The maximum lateral loads that a masonry infill panel can resist.

Infilled Frame: Lateral and vertical load resisting structural systems that consist of frame and infill panels. The infill can be full, partial, or contain openings.

Isolated Masonry Infill Panel: A specific type of masonry infill panel in which the panel and the confining frame are in direct contact at the panel base only. The other three panel sides are not in contact with the frame.

Laminate: One or more layers of fiber, bound together in a resin matrix.

Life Safety Performance Level: Building performance that includes significant damage to both structural and nonstructural components during an earthquake, though at least some margin against either partial or total structural collapse remains. Injuries may occur, but entrapment is low.

Masonry Infill Panel: A masonry wall constructed within an existing confining frame. These panels are built in-place and should be constructed so that there is full contact along the entire perimeter of the infill.

Matrix: The resin or polymer material in which the fibers of the composite are embedded.

Moment Hinge: A plastic hinge defined to model the inelastic action of a structural member when its yield strength is surpassed due to bending moment forces.

Mortar Joint: A mixture of sand, cement, lime, and water that is used to bond masonry units together.

Net Fiber Area: The area of the FRP system excluding resin.

Plastic Hinge: Location of inelastic action on a structural member.

Plies: Number of layers of FRP.

Polymer: Any of numerous natural and synthetic compounds of usually high molecular weight consisting of repeated linked units, each a relatively light and simple molecules.

Resin: The mixed polymer component or matrix of the FRP.

Rigid End Offset: The length of a structural member assumed to be completely rigid in order to model the effects of full contact between the infill and structural members.

Shear Hinge: A plastic hinge defined to model the inelastic action of a structural member when its yield strength is surpassed due to shear forces.

Solid Infill Panel: A masonry infill panel built with solid masonry units (such as clay brick).

Structural Adhesive: A resinous bonding agent used to transfer loads between the concrete substrate and FRP.

Ultimate Load: The maximum value of base shear predicted by a nonlinear structural pushover analysis.

Yield Load: Value of base shear on a bilinear estimate of a pushover curve at which the slope changes and the model becomes more flexible.

Symbols

a	Equivalent width of infill strut (in.)
a_{mod}	Modified equivalent width of infill strut (in.)
A_f	Area of FRP on the tension face of the member (sq in.)
A_{fv}	Area of FRP shear reinforcement within spacing s_f (sq in.)
A_g	Gross cross sectional area of confining frame elements (sq in.)
A_n	Net cross sectional mortar/grouted area of infill panel along its length (sq in.)
A_{open}	Total area of openings in a selected infill panel (sq in.)
A_{panel}	Gross area of an infill panel (sq in.)
A_s	Area of reinforcing steel in tension (sq in.)
A'_s	Area of reinforcing steel in compression (sq in.)
A_{st}	Total area of longitudinal reinforcing steel in a column (sq in.)
b	Width of the concrete member (in.)
c	Depth to the neutral axis (in.)
C	A multiplication factor for calculating strut width that accounts for aspect ratio
C_E	Environmental Reduction Factor
d	Depth to the centroid of the reinforcing steel in tension (in.)
d'	Depth to the centroid of the reinforcing steel in compression (in.)
d_f	Depth of the FRP shear reinforcement (in.)
d_m	Nonlinear drift associated with the masonry infill panel (%)
D	Diagonal length of infill (in.)
E_c	Modulus of elasticity of the confining frame (ksi)

E_{f1}	Initial modulus of elasticity of the FRP system (ksi)
E_{f2}	Secondary modulus of elasticity of the FRP system (ksi)
E_m	Modulus of elasticity of masonry in compression (ksi)
E_s	Modulus of elasticity of the reinforcing steel (ksi)
f_c	Maximum concrete stress at M_y (ksi)
f'_c	Concrete compressive strength at 28 days (ksi)
f'_{cc}	Confined concrete compressive strength (ksi)
f_{fe}	Effective stress in the FRP (ksi)
f_{fu}	Design ultimate tensile strength of the FRP system (ksi)
f'_{fu}	Ultimate tensile strength of the FRP system determined from testing (ksi)
f_{fy}	Design yield stress of the FRP system (ksi)
f'_{fy}	Yield stress of the FRP system determined from the bilinear FRP stress-strain curve (ksi)
f_l	Confining pressure due to FRP jacket (ksi)
f'_m	Compressive strength of masonry (ksi)
f_s	Stress in the tension reinforcing steel (ksi)
f'_s	Stress in the compression reinforcing steel (ksi)
f'_t	Masonry flexural tensile strength (ksi)
f'_v	Masonry shear strength (ksi)
f_y	Yield stress of the reinforcing steel (ksi)
G_m	Masonry shear modulus ($0.4 E_m$) (psi)
h	Height of the concrete member (in.)
h_m	Height of the masonry infill panel (in.)
h_m/t	Masonry infill panel slenderness ratio
$h_{opening}$	Height of individual infill opening (in.)
H	Height of the confining frame (in.)
I_{beam}	Moment of inertia of confining beam (in ⁴)
I_{column}	Moment of inertia of confining column (in ⁴)
I_{frame}	Lesser Moment of inertia between I_{beam} and I_{column} (in ⁴)
$IP_{capacity}$	Ultimate in-plane loading capacity (kips)
$IP_{reduced}$	Reduced in-plane loading capacity resulting from out-of-plane forces (kips)
k_1	Concrete strength modification factor applied to κ_v
k_2	FRP wrapping scheme modification factor applied to κ_v
K_i	Modified initial bilinear stiffness (k/in.)
K_f	Modified post-yield bilinear stiffness (k/in.)
K_{SSC}	Initial bilinear stiffness as estimated from Stafford-Smith and Carter (1969) (k/in.)
K_y	Initial bilinear stiffness as estimated from Mainstone (1971) (k/in.)

K_u	Post-yield bilinear stiffness as estimated from Mainstone (1971) (k/in.)
l	Length of the infill panel (in.)
l/h_m	Infill panel aspect ratio
l_{beam}	Distance from the face of the beam to the first beam plastic hinge (in.)
l_{column}	Distance from the face of the column to the first column plastic hinge (in.)
L_e	FRP bond length (in.)
L_f	Length of the confining frame (in.)
$L_{opening}$	Length of individual infill opening (in.)
M_n	Nominal moment capacity (k-in.)
M_{ult}	Moment demand based on factored loads (k-in.)
M_y	Flexural yield strength of the beam (k-in.)
n	Number of plies of FRP
OP_{demand}	Out-of-plane load that a structure is required to withstand (kips)
$OP_{capacity}$	Out-of-plane load that a structure is capable of withstanding (kips)
P_n	Nominal axial compression capacity (kips)
P_{ult}	Compressive axial demand based on factored loads (k-in.)
r	Radius of the edges of a square or rectangular section (in.)
R_{cr}	Force required to reach the masonry infill panel's crushing strength (kips)
R_{shear}	Force required to reach the masonry infill panel's shear strength (kips)
R_{strut}	Minimum of R_{cr} and R_{shear} (kips)
$(R_1)_i$	In-plane reduction factor that accounts for the presence of infill openings
$(R_1)_o$	Out-of-plane reduction factor that accounts for the presence of infill openings
$(R_2)_i$	In-plane reduction factor that accounts for existing panel damage
$(R_2)_o$	Out-of-plane reduction factor that accounts for existing panel damage
$(R_3)_o$	Out-of-plane reduction factor that accounts for the flexibility of the confining frame
s_f	Spacing of FRP shear reinforcement (in.)
t	Gross thickness of the infill (in.)
t_{eff}	Effective net thickness of the infill (in.)
t_f	Thickness of the FRP system (in.)
T_n	Nominal axial tension capacity (kips)
T_{ult}	Axial tension demand based on factored loads (kips)
V_c	Shear strength of the concrete (kips)
V_f	Shear strength of the FRP (kips)
V_n	Nominal shear capacity (kips)
V_s	Shear strength of the reinforcing steel stirrups (kips)
V_u	Ultimate capacity of a structure as computed by a pushover analysis (kips)
V_{ult}	Shear demand based on factored loads (k-in.)

V_y	Estimated bilinear “yield” strength of a structure (kips)
w	Parameter used in the out-of-plane strength evaluation of masonry infill panels (ksi)
w_f	Width of the FRP strip used for shear strengthening (in.)
α	Inclination angle of FRP shear reinforcement (degrees)
β_I	Ratio of the depth of the equivalent rectangular stress block to the depth of the neutral axis
δ	Out-of-plane infill deflection at the center (mid-height) of the panel (in.)
Δ	In-plane lateral deformation experienced by the structure (in.)
Δ_u	Bilinear deflection at ultimate load as computed by a pushover analysis (in.)
Δ_y	Estimated bilinear “yield” deflection (in.)
Δ_u'	Modified bilinear deflection at ultimate load (in.)
Δ_y'	Modified bilinear “yield” deflection (in.)
ϵ_{bi}	Strain level in the concrete substrate at the time of FRP installation (in./in.)
ϵ_c	Maximum concrete strain at M_y (in./in.)
ϵ_{cr}	Ultimate crushing strain of masonry (in./in.)
ϵ_{cu}	Maximum usable compressive strain in the concrete (in./in.)
ϵ_{fe}	Effective strain in the FRP at failure (in./in.)
ϵ_{fu}^*	Ultimate rupture strain of the FRP system determined from testing (in./in.)
ϵ_{fu}	Design rupture strain of the FRP system (in./in.)
ϵ_{fy}	Design yield strain of the FRP system (in./in.)
ϵ_{fy}^*	Yield strain of the FRP system determined from the bilinear FRP stress-strain curve (in./in.)
ϵ_s	Strain in the tension reinforcing steel (in./in.)
ϵ'_s	Strain in the compression reinforcing steel (in./in.)
ϵ_y	Yield strain of the reinforcing steel (in./in.)
ϵ_y	Yield strain of the reinforcing steel (in./in.)
κ_a	Efficiency factor for confinement
κ_m	Bond-dependent coefficient for flexure
κ_v	Bond-dependent coefficient for shear
λ_o	Parameter required to evaluate the out-of-plane infill strength
λ_I	Relative infill-to-frame stiffness parameter
ϕ	Strength reduction factor
ϕ_n	Curvature in the beam at M_n (rad/in.)
ϕ_y	Curvature in the beam at M_y (rad/in.)
ρ_f	FRP reinforcement ratio
ρ_g	Longitudinal steel reinforcement ratio
θ	Angle of the concentric equivalent strut (degrees)

θ_{beam}	Angle between face of the eccentric equivalent strut and the horizontal if the strut were to be modeled eccentrically along the beam (degrees)
θ_{column}	Angle between face of the eccentric equivalent strut and the horizontal if the strut were to be modeled eccentrically along the column (degrees)
θ_{strut}	Angle made between the eccentric equivalent strut and the horizontal if the strut is modeled as a centerline element (degrees)
ξ_1	FRP strength increase factor
ξ_2	FRP stiffness increase factor
ψ_f	Additional FRP reduction factor

CERL Distribution

Chief of Engineers

ATTN: CEHEC-IM-LH (2)

ATTN: CECW-EW (2)

Engineer Research and Development Center (Libraries)

ATTN: ERDC, Vicksburg, MS

ATTN: Cold Regions Research, Hanover, NH

ATTN: Topographic Engineering Center, Alexandria, VA

Defense Tech Info Center 22304

ATTN: DTIC-O

7

5/02

REPORT DOCUMENTATION PAGE

Form Approved
OMB No. 0704-0188

Public reporting burden for this collection of information is estimated to average 1 hour per response, including the time for reviewing instructions, searching existing data sources, gathering and maintaining the data needed, and completing and reviewing this collection of information. Send comments regarding this burden estimate or any other aspect of this collection of information, including suggestions for reducing this burden to Department of Defense, Washington Headquarters Services, Directorate for Information Operations and Reports (0704-0188), 1215 Jefferson Davis Highway, Suite 1204, Arlington, VA 22202-4302. Respondents should be aware that notwithstanding any other provision of law, no person shall be subject to any penalty for failing to comply with a collection of information if it does not display a currently valid OMB control number. PLEASE DO NOT RETURN YOUR FORM TO THE ABOVE ADDRESS.

1. REPORT DATE (DD-MM-YYYY) 12-2002		2. REPORT TYPE Final		3. DATES COVERED (From - To)	
4. TITLE AND SUBTITLE Design of Fiber-Reinforced Polymer Materials for Seismic Rehabilitation of Infilled Concrete Structures				5a. CONTRACT NUMBER	
				5b. GRANT NUMBER	
				5c. PROGRAM ELEMENT NUMBER	
6. AUTHOR(S) Ghassan K. Al-Chaar and Gregory E. Lamb				5d. PROJECT NUMBER 622784AT41	
				5e. TASK NUMBER	
				5f. WORK UNIT NUMBER 0083B7	
7. PERFORMING ORGANIZATION NAME(S) AND ADDRESS(ES) U.S. Army Engineer Research and Development Center (ERDC) Construction Engineering Research Laboratory (CERL) PO Box 9005 Champaign, IL 61826-9005				8. PERFORMING ORGANIZATION REPORT NUMBER ERDC/CERL TR-02-33	
9. SPONSORING / MONITORING AGENCY NAME(S) AND ADDRESS(ES) U.S. Army Corps of Engineers 441 G Street, NW Washington, DC 20314-1000				10. SPONSOR/MONITOR'S ACRONYM(S) CECW-EW	
				11. SPONSOR/MONITOR'S REPORT NUMBER(S)	
12. DISTRIBUTION / AVAILABILITY STATEMENT Approved for public release; distribution is unlimited.					
13. SUPPLEMENTARY NOTES Copies are available from the National Technical Information Service, 5285 Port Royal Road, Springfield, VA 22161.					
14. ABSTRACT <p>Of the government buildings located in high- or moderate-risk seismic zones, more than half were found vulnerable to damage during an earthquake. One rehabilitation technique that addresses vulnerabilities in both the masonry infills and in nonductile concrete frames is using fiber-reinforced polymer (FRP). An experimental program was conducted on reinforced concrete (R/C) frames infilled with masonry. Based on this research and related research in the field, this report was developed to provide in-depth guidelines for engineers and practitioners on how to evaluate the strength and stiffness of R/C members and masonry-infilled frames strengthened with FRP.</p> <p>The report's information was compiled and written following a logical sequence intended to help the engineer in the evaluation process. The second chapter outlines the steps that must be followed to obtain all the required material and geometrical properties of the structure to be evaluated. The following chapters present the load and deformation characteristics of R/C members strengthened with FRP. Next, the in-plane strength and stiffness evaluation procedures are shown for the lateral-force resisting system consisting of infilled frames rehabilitated with FRP. The illustrative example in Appendix A summarizes the entire evaluation process, and Appendix B is a commentary on selected sections of the report.</p>					
15. SUBJECT TERMS infilled concrete structures, seismic vulnerability, reinforced concrete (R/C), fiber-reinforced polymer (FRP), lateral force, structural reliability, masonry, structural engineering					
16. SECURITY CLASSIFICATION OF:			17. LIMITATION OF ABSTRACT SAR	18. NUMBER OF PAGES 83	19a. NAME OF RESPONSIBLE PERSON Ghassan K. Al-Chaar
a. REPORT Unclassified	b. ABSTRACT Unclassified	c. THIS PAGE Unclassified			19b. TELEPHONE NUMBER (include area code) (217)373-7247